INVESTIGATIONS OF ELECTRONIC AND PHONON MEDIATED SUPERCONDUCTIVITY OF Rb and K DOPED GRAPHENE

Gebrekirstos Gebreamlak Berhe

A Thesis Submitted to

The Materials Science Program

Presented in Partial Fulfillment of the Requirements for the

Degree of Master of Science (Materials Science)

Addis Ababa University

Addis Ababa, Ethiopia

June 20 (2013)

Addis Ababa University

School of Graduate Studies

This is to certify that the thesis prepared by Gebrekirstos Gebreamlak Berhe, entitled: *Investigations of Electronic and Phonon Mediated superconductivity of Rb and K doped graphene* and submitted in partial fulfillment of the requirements for the degree of Degree of Master of Science (Materials Science) complies with the regulations of the University and meets the accepted standards with respect to originality and quality.

Signed by the Examining Committee

Examiner: Prof. Teketel Yohannes Signature _____ Date 04/07/2013

External Examiner: Dr. Ahmed Mustefa Signature _____ Date _____

Advisor: Prof. Javed Mazher Signature _____ Date 04/07/2013

Prof. Teketel Yohannes

Chair of Deparment

Abstract

INVESTIGATIONS OF ELECTRONIC AND PHONON MEDIATED SUPERCONDUCTIVITY OF (Rb, K) DOPED GRAPHENE

Gebrekirstos Gebreamlak

Addis Ababa University, 2013

We performed ab-initio calculations on a novel class of superconductors, which comprise of alkali doped graphene. The graphene is doped with the potassium and rubidium atoms. We theoretically studied lattice dynamics by performing density functional perturbation theory based simulations for studying doping effects on graphene's phonon modes. Spectra of electronic and phonon density of states are compared in between undoped and K and Rb doped graphene. Besides, the study of electron-phonon interactions is also performed and the significant amount of electron-phonon coupling is found to be present among the K and Rb doped graphene. That is attributed as one of the reasons for as-found induced superconductivity at certain crystal symmetry points of interest in Brillouin zone of this material, specifically, at the (Γ and $\mathbf{K}$) points. The higher values of electron-phonon couplings of 0.3679 and 0.1907 correspondingly for the potassium and rubidium doped graphene are found to be responsible for the superconductivity. Nevertheless, during our calculations the el-ph coupling strengths for pristine graphene is always found to be zero at various special points. In addition, the prospects of the phenomena of superconductivity amongst the alkali doped graphene are discussed in detail.

Acknowledgments

First and foremost I thank the almighty God, next I would like to express my sincere thanks to my advisor and instructor Professor Javed Mazher for his guidance, assistance, and contribution of valuable suggestions. I would like also to thank the Addis Ababa University Graduate Studies Program for giving me the chance to join the Materials Science Masters program. And I would like to extend my acknowledgement to the Materials Science Program specifically Professor Teketel Yohannes for providing me all the facilities required for this thesis. I would like also to thank to all my family for their contineuos assistance to persue my education., I would like to thank my classmates Mesfin Haile , Fetene Fufa and Asegidew Ergetie for their cooperation. At last I would like to thank Ms Azeb Tesfay for her contributions on this thesis.

Contents

List of Figures

List of Tables

Chapter 1

Introduction

Graphene, a wonder two dimentional material that is responsible for the Nobel Prize for Andre Geim and Konstantin Novoselov (2010) in Physics, has many remarkable nanoscopic properties except superconductivity. However, it is an ideal material for the phenomena of superconductivity related high speed electronics due to the presence of fast charge carrier dynamics. Hence, the induction of superconductivity among graphene based nanomaterials has been the focus of most of the recent research effrots [1]. In this thesis, we doped the graphene surface with alkali metal atoms (Rb and K) and thus the phonon mediated superconductivity is found to be induced. Graphene is among the most prominent nanoscale materials currently studied. It is a zero gap semiconductor and is the physical realization of many fundamental concepts and phenomena in solid-state physics [1]. Thus a modest attempt has been made in the direction of appending the list of graphene's many remarkable properties, in which the superconductivity is notably found to be absent. Nevertheless, it is quite possible to induce superconductivity in this class of materials, we have tried to use the route of alkali atom's proximity with the graphene supercell [1]. In this work, the adsorption of two different metal adatoms on graphene is studied using first-principles density functional theory (DFT) and quantum espresso software, (PWscf and PHonon) packages.

The organization of this this is as follows. Chapter one deals with the

informations to the basic concepts about graphene, its novel properties, and literature survey on the recent scientific research on alkali doped graphene. Chapter two describes the objectives of this thesis and chapter three is about the review on theoretical techniques used in the computational materials science. Chapter four is the methodology adopted for the evaluation of superconductivity within density functional theory and density functional perturbation theory framework. Finally, fifth and sixth chapters discuss about the results and conclusions of this work, respectively.

1.1 Graphene

Graphene is a single two-dimensional (**2D**) monolayer of carbon atoms bound in a hexagonal lattice structure [2]. It is a basis for other graphitic materials like wrapped graphene (**0D** fullerene), rolled graphene (**1D** CNTs) and stacked graphene (**3D**) graphite.

It has been extensively studied in the last several years eventhough it was only isolated for the first time in 2004 [2]. Andre Geim and Konstantin Novoselov won the 2010 Nobel Prize in Physics for their ground breaking work on graphene. The fast uptake of interest in graphene is due to exceptional properties that it has been found to possess.

Band structure is most often studied from a stand point of the relationship between the energy and momentum of electrons with in a given material. Since the graphene constrains the motion of electrons to two dimensions, the momentum space is also constrained to two dimensions. Graphene's zero gap semiconductivity is because the conduction and valence bands meet at the Dirac points Figure 1.1. The π and $\pi*$ bands touch at the corners of the hexagonal brillouin zone. These brillouin zone corners are their momentum vectors usually denoted by K and K' (Figure 1.1). The graphene sheet is highly specific for this linear momentum relation.

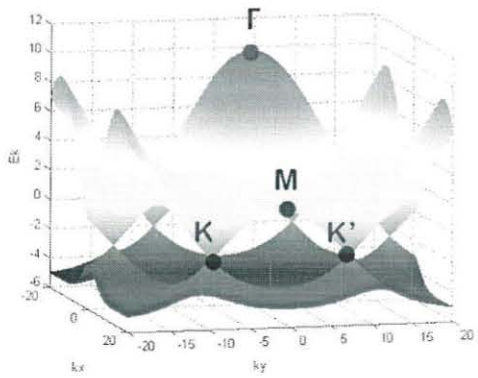

Figure 1.1: *First Brillouin zone and band structure of graphene.* Γ *is the zone center. K and k' are the Dirac points. [2]*

The electronic group velocity, estimated at the Dirac points is approximately $1 \times 10^6 m/s$ [3]. Hence, graphene exhibits elecronic properties of the form Dirac equation. Since the bonding and antibonding σ bands have large energy gap($>$ 10 eV at Γ), this points are frequently neglected in electronic calculations since they are far away from the Fermi level to participate in this. Therefore the remaining two π bands are responsible to describe the elecronic properties of graphene.

The electronic wavefunctions from different atoms of graphene are overlap. But the overlap between p_z orbitals and the s , p_x and p_y orbitals forbids by symmetry. Therefore the π bands in graphene, can be treated independently from the other valence electrons.

In traditional semiconductors the primary point of interest is generally Γ, where momentum is zero. Electrons within about 1 eV of the Dirac energy have a linear dispersion relation. The linear dispersion relation is well-described by the Dirac equation for massless fermions. that is, the effective mass of the charge carriers in this region is zero.

1.2 Superconductivity

Superconductivity is mostly characterized by a vanishing electrical resistance below a certain temprature T_c, called critical temprature [4]. Below T_c there is no measurable DC resistance in a superconductor, and if a current is set up in it, it will flow without dissipation practically forever. Experiments trying to give estimates that it is constant $10^6 - 10^9$ years! [4].

Thus, the superconducting state is not a state of merely very low resistance, but one with a truly zero resistance. For typical supercconductors T_c, is in the range of a few degrees kelvin, which has made it difficult to take advantage of this extraordinary behavior in practical applications is quite difficult.

In 1986 a new class of superconducting materials was discovered by Bendnortz and Muller, dubbed high-temprature superconductors, in which the T_c is much higher than in typical supercconductors: in general in the range of 90 k [4]. This is well above the freezing point of N_2(77 k), so that this much more abundant and cheap substance can be used as the coolant to bring the superconducting materials below their critical point. The low temperature supercconductor are called conventional supercconductors to distinguish them from the high temperature kind.

In some metals for example, the superconducting state occurs due to the presence of a 10^{-4} fraction of "abnormal" electrons, while the other 99.99 free (conduction) electrons remain absolutely normal. The correlated behavior of the small fraction of these "abnormal" electrons overwhelms the rest. Due to the presence of these "abnormal" electrons, the metal is no longer a metal but a superconductor, losing its ability to resist to a small-magnitude electrical current. The presence of normal (conduction) electrons is completely masked by that of the "abnormal" electrons, as if the normal electrons were not existing at all. (Of course, we talk only about electron transport properties of a metal, the crystal structure of a metal is almost unchanged below the critical temperature, i.e. when a metal becomes superconducting.

1.2.1 Bardeen, Cooper and schrieffer (BCS) theory of superconductivity

There are two main ingriedients in the microscopic theory of superconductivity developed by Bardeen, Cooper and schrieffer (BCS). The first is an effective attractive interaction between two electrons that have opposite momenta and opposite spins, which leads to the formation of the so called "cooper pairs" [4]. The second is the condensation of the cooper pairs into a single state which is called the "superconducting condensate", this is the state responsible for all the manifestations of superconducting behavior.

Cooper pairing

The Coulomb interaction between two electrons is of course repulsive. For two free electrons at a distance r, the interaction potential in real space is

$$V(\mathbf{r}) = \frac{e^2}{|\mathbf{r}|} \tag{1.1}$$

We can think of the interaction between two free electrons as a scattering process corresponding to the exchange of photons, the carriers of the electromagnetic field: an electron with initial momentum $\hbar\,\kappa$ scatters off another electron by exchanging a photon of momentum $\hbar\,\kappa$. Due to momentum conservation, the final momentum of the electron will be $\hbar\,k = \hbar(k-q)$. We can calculate the matrix element corresponding to this scattering of an electron, taking to be in plane wave state

$$\langle k'|V|k\rangle = \frac{1}{\Omega}\int e^{-i(k-q).r}V(r)e^{ik.r}dr = \frac{4\pi e^2}{|q|^2} \tag{1.2}$$

the last expresion being simply the Fourier transform $V(q)$ of the bare coulombic potential with $q = k - k'$.

The preceding discusion concerned the interaction between two electrons in a solid assuming that the ions are fixed in space. When the ions are allowed to

move, a new term in the interaction is introduced. We can describe this motion interms of phonons emitted by the travelling electron. The effective interaction between electrons due to exchange of phonon is given in reciprocal space by

$$V_{kk'}^{phon}(q) = \frac{g^2 \hbar w_q}{(\in_{k'} - \in_k)^2 - (\hbar w_q)^2} \tag{1.3}$$

where k, k' and $\in_k$, $\in_{k'}$ are the incoming and outgoing wave-vectors and energies of the electrons, and q, $\hbar w_q$ is the wave vector and energy of the exchanged phonon, g is a constant that describes the strength of the electron-phonon interaction.

1.2.2 Carbon based systems superconductivity

Superconductivity in carbon based systems has been studied substantially over the last ten years. Graphene and carbon nanotubes **"CNTs"** are among the most prominent nanoscale materials currently studied. The confinement to one or two dimensions and the high symmetry of these materials lead to interesting new physics and many potential applications, especially involving the electronic structure and transport properties [5]. Diamond becomes [6] superconducting when doped with boron. Graphite and fullerene are superconducting when intercalated with alkali atoms with a record breaking $T_c = 39\ K$ [6].

Metals adsorbed on nanoscale carbon surfaces have been shown experimentally to form a variety of structures, such as contineuos coatings or discrete clusters, and these structures can be manupulated to give rise to interesting new phenomena. For example, experiments have demonstrated the ability to control metal clusters on CNTs surfaces [5]. It is well known that the phonon- mediated attractive electron-electron interaction leads to a superconductive instability in 2D and 3D conductors. In CNTs, which is one of typical 1D conductors, a variety of 1D quantum phenomena have been reported. However, intrinsic superconductivity has been reported in the CNTs only by a few groups [7].

1.2.3 Graphene based superconductivity

As the theory has been developed to describe the behaviour of two-dimensional electron gases hosted in conventional semiconducting heterostructures, for which it works quantit

atively with impressive accuracy, the unexpected behaviour observed in graphene suggests that this material is fundamentally different. Indeed, it is now understood that the anomalous behaviour of graphene originates from the fact that, at low energy, the dynamics of electrons is governed by the relativistic Dirac equation for massless particles, rather than the conventional Schrodinger equation [8].

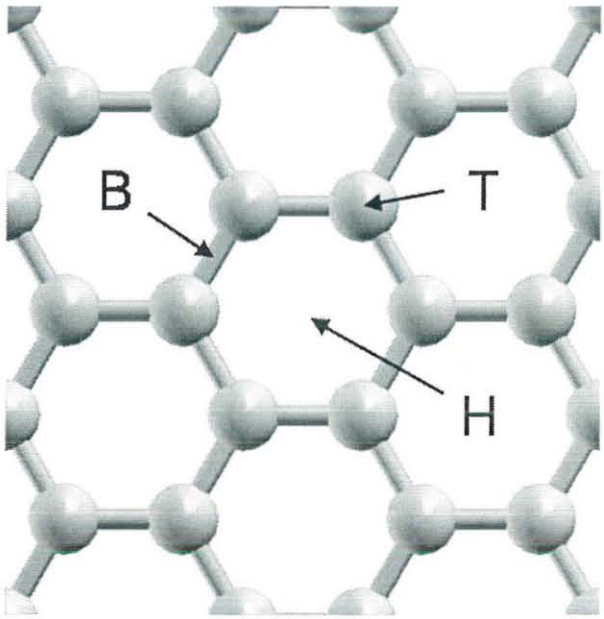

Figure 1.2: *The three adsorption sites considered:hollow (H), bridge (B) and top (T)*

For adsorption of adatoms on graphene, there are three sites, the hollow (**H**) site at the center of hexagon, the bridge (**B**) site at the mid point of carbon-carbon bond and the top (**T**) site directly above the carbon atom Figure 1.2 [5].

Metal adatoms from groups **I -III** all bind most strongly to the **H** site. For the alkalis, the relatively high ratio of adsorption energy to bulk cohesive energy suggest that alkali are able to form $2D$ layers on the surface of graphene, in agreement with experiments observing $2D$ alkali layer formation on graphite. Since graphene is not superconductor, phonon-mediated superconductivity must be induced by an enhancement of the electron-phonon coupling (λ) [1].

$$\lambda = \frac{N(0)D^2}{M\omega_{ph}^2} \tag{1.4}$$

where, $\mathbf{N(0)}$ is the electronic density of states per spin (DOS) at the Fermi level, **D** is the deformation potential, **M** and ω_{ph} are the effective atomic mass and phonon frequency.

Table 1.1: *Lattice constant (a), adatom–graphene distance (h) in Å, electron–phonon coupling (λ), logarithmic frequency average ($w_{log} cm^{-1}$) and Tc in Kelvin for CaC_6 and LiC_6 systems.[1]*

		a	h	λ	w_{log}	T_c
CaC_6	Bulk	4.30	2.19	0.68	284.3	11.5
CaC_6	Mono	4.26	2.24	0.40	309.9	1.4
LiC_6	Bulk	4.29	1.83	0.33	715.7	0.9
LiC_6	Mono	4.26	1.83	0.61	277.8	8.1

In undoped graphene, λ is small and phonon mediated supercconductor does not occur as small number of carries leads to vanishinglly small $\mathbf{N(0)}$. To induce superconductivity could then be to fill by rigid -band doping the carbon π-states to have enough carrier.

However besides the fact the π-DOS grows very slowly with doping, its impact will be hidered by two major difficulities. First, even if the deformation potential related to coupling between π-bands and in-plane phonon vibrations is large and and leads Kohn anomalies, these vibrations are highly energetic (ω_{ph} $\approx 0.16eV$) [1]. Second, symmetry forbids the coupling between π-states and softer out-of-plane phonon vibrations.

To promote coupling to carbon out-of-plane vibrations, it is necessarly to promote new electronic states at the Fermi level as happens in GICs. In GICs, the larger T_c is indeed obtained when the distance (h) is smaller because $\mathbf{D}$ increases.

Following these accepted guide lines for GICs, we explore the possibility to induce superconductivity in graphene by foreign atom coverage.

Calcium, as is the case for other alkali metals, adsorbs in the hollow sites of graphene Figure 1.3 and Table 1.1 [1]. The electronic band structure of Lithium-doped graphene is reported in Figure 1.4.

Electron-Phonon interaction in graphene

For simple systems with isotropic electronic structures, electron-phonon interaction can be characterized by the Eliashberg spectral function $\alpha^2F(\omega)$ which describes the energy of the phonon modes involved as well as their coupling strengths.

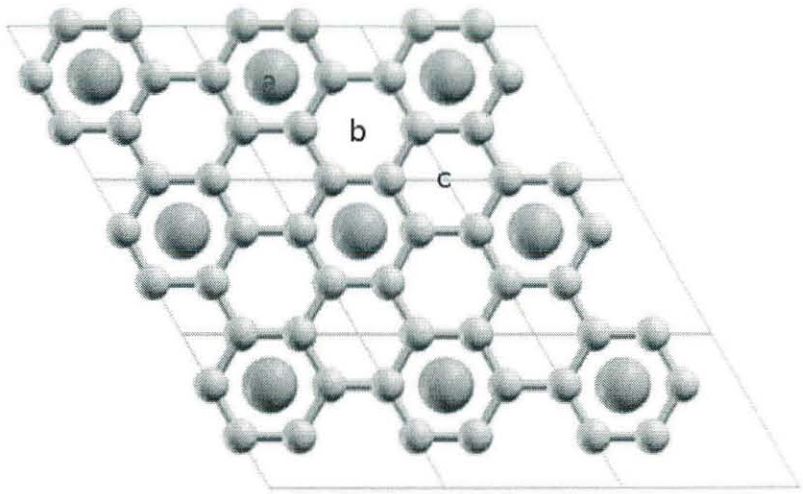

Figure 1.3: *The adatoms sit in the hollow sites of the graphene layer. For each graphene layer, the calcium atoms occupy different hollow sites of the three allowed in the in-plane unit cell [1].*

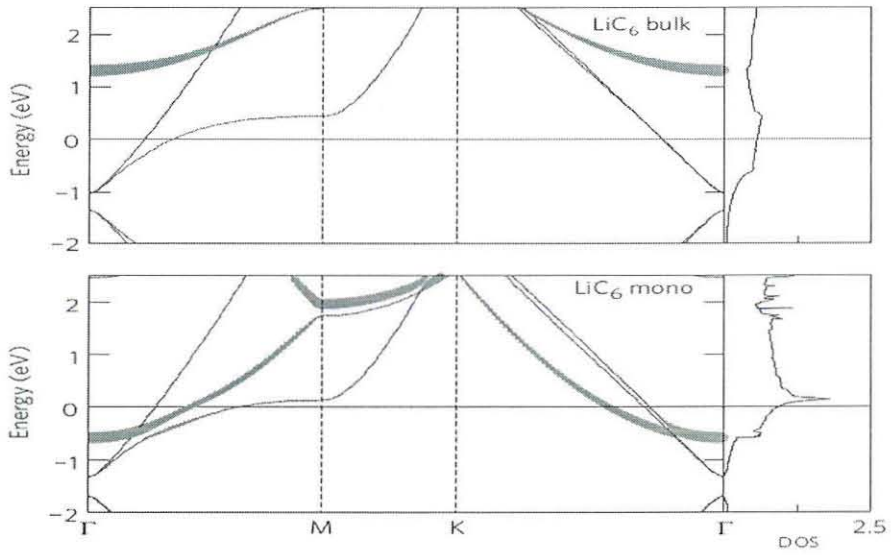

Figure 1.4: *From top to bottom: band structure and total density of states per spin (DOS) of LiC_6 bulk and LiC_6 monolayer. The Dirac point is folded at the Γ-point at -1.56 eV [1].*

It played a crucial role in establishing the BCS theory of superconductivity. It is clear that one can expect very interesting new properties of the superconductivity in the visinity of the Dirac points. However, this region is least favorable for the existence of superconductivity due to the very low density of states, and one should tune the Fermi energy away from the Diracpoints in order to have a hope to obtain

superconductivity.

By using results of numerical calculations for the interactions obtained for the normal state, the transition temprature, T_c, is estimated and superconductivity is possible with T_c of the order of several Kelvin. Most favorable is a singlet pairing between different valley.

The hamiltonian describing the electron-phonon system can be written in a general form

$$\hat{H} = \hat{H}_0 + \hat{H}_{e,ph} + \hat{H}_{e,e} \tag{1.5}$$

where

$$\hat{H}_0 = \sum_{\mathbf{p},\sigma} (\varepsilon(\mathbf{p}) - \mu) C^+_{p,\sigma} C_{p,\sigma} \tag{1.6}$$

is the operator of the kinetic energy, $\varepsilon(\mathbf{p})$ is the spectrum of the non-interacting electrons, μ is chemical potential (Fermi energy at low temperature), σ is the spin index, $C_{\mathbf{p},\sigma}(C^+_{\mathbf{p},\sigma})$ is the electron annihilation(creation) operator for the electron with momentum $\mathbf{p}$ and spin σ, $\hat{H}_{e,ph}$ stands for the electron-phonon interaction and $\hat{H}_{e,e}$ for the electron-electron one.

The key factors determining the electron-phonon coupling strength are the density of states around the Diracpoint energy and the electron-phonon matrix elements between the initial and the final electronic states close to the Fermi level [5]. The density of states of pristine graphene has a finite density of state. Despite this difference, at low doping with only one band occupied ($|E_F - E_D| < 0.2\ eV$, E_D being the energy at the energy at the Dirac point and is set to $E_D = 0$ in the following discusion), the electron-phonon coupling strength in bilayer graphene. This indicates that as in graphene, there is no significant scattering between low energy elecronic states in bilayer graphene and in graphite arising from the chiral nature of the charge carriers in bilayers graphene and in graphite i.e, it is a matrix element effect.

In order to determine which phonon modes lead to the differences in the electron-phonon coupling strengths between monolayer and biylayer graphene, we

decompose the coupling strength $\lambda_{n\kappa}$ of both systems in to contributions from each phonon branch and wave vector.

Phonon dispersion relations

The phonon energy spectrum is important for determining the sound velocity, phonon density of states, phonon-phonon or electron-phonon scattering rates, lattice heat capacity, as well as the phonon thermal conductivity. The optical phonon properties manifest themselves in Raman measurements. The number of graphene layers, their quality and stacking order can be clearly distinguished using the Raman spectroscopy. For these reasons, significant efforts have been made to accurately determine the phonon energy dispersion in graphene and to reveal specific features of their phonon modes.

Graphene has six phonon polarization branches, these are, (i) out-of-plane acoustic (ZA) and out-of-plane optical (ZO) phonons with the displacement vector along the Z axis; (ii) transverse acoustic (TA) and transverse optical (TO) phonons, which corresponds to the transverse vibrations within the graphene plane; (iii) longitudinal acoustic (LA) and longitudinal optical (LO) phonons, which corresponds to the longitudinal vibrations within the graphene plane.

1.2.4 Applications of graphene based superconductivity

Non superconductiveness of graphene makes it less choice for practical low temprature and high magnetic field applications. But if it is possible to find a way to induce superconductivity, it could improve the performance and enable more efficient integration of a variety of promising device concepts including:

- nanoscale superconducting quantum interference devices [1].
- single-electron superconductor–quantum dot devices [1].
- nanometre-scale superconducting transistors [1].
- cryogenic solid-state coolers [1].

The zero excitation energy near the Dirac points of graphene has a linear Dirac-type energy spectrum near each six Dirac points. Unlike a normal metal, in graphene the energy of injected electron can be easily and efficiently controlled by a gate voltage [9] , which is very usefull in studies of the charge transfer through graphene based junctions. It was also shown that by changing the Fermi energy, E_F, via the gate voltage, graphene-based superconductor junctions can be exhibit unique local and non-local specular Andreev reflections. This new type of reflections takes place in the weakly doped graphene.

Chapter 2

Objectives

2.1 General Objectives

• To induce superconductivity on graphene by doping its surface with rubidium and potassium adatom.

2.2 Specific Objectives

• Optimizing the geometry of the supercell of graphene and doped graphene.

• Using ATK and Quantum Espresso-DFT method investigate the electronic properties of pristine graphene.

• Calculate the electronic band structure and DOS of potassium and rubidium doped graphene.

• Calculate the phonon-mediated superconductivity of this doped nanoscale material.

Chapter 3

Computational Review

Since the discovery of electron(1896), the theory of electron in materials become challenging task, because electron is quantum glue that hold all the quantum things that include electronic, optical, magnetic, mechanical etc properties of materials. The field of electronic structure is at a momentous stage, with basic advances in basic theory, new algorithms, and computational methods. It is now feasible to determine many properties of materials directly from the fundamental equations for the electrons and to provide new insights into vital problems in physics, chemistry, and materials science. Increasingly electronic structure calculations are becoming tools used by both experimentalists and theorists to understand characteristic properties of matter and to make specific predictions for real materials and experimentally observable phenomena [10]. There is a need for coherent, instructive material that provides an introduction to the field and a resource describing the conceptual structure, the capabilities of the methods, limitations of current approaches, and challenges for the future [11].

3.1 Historical Background

In 1890 Lorentz propose the first theory in materials science that is Maxwell theory of electromagnetism to find electronic and magnetic properties of matter. After these, Zeeman (1896) find atomic spectra splitting and explain in by Lorentz

electronic theory. Then after J.J Thomson (1897) discovery charge to mass ratio. Bohr (1911) made foundational contributions to understanding atomic structure and quantum mechanics, for which he received the Nobel Prize in Physics in 1922. This idea explain the atomic spectra is discrete. Wolfgan Pauli and Arnold sommerfield show that:

• Weak paramagnetism can be explained by spin polarization of electrons or fermi Dirac statistics.

• At a temrature of zero Kelvin (0k) and at a magnetic field of zero tesla (0T), electrons get spin paired and fill the lowest energy

state up to Fermi energy leaving all other states above E_F empty.

• For non zero temperatures and non zero magnetic field only the electronic states near the Fermi level are able to participate in electric conduction, thermal conduction, in paramagnetism and other properties.

The theory of materials science has seen many historical developments since these early breakthroughs. The use of quantum mechanics for the complete description of quantum particles' behaviour inside the advanced materials is one of them. That is widely used in the past few decades to explore the novel properties among zero, one, two dimensional nanomaterials.

3.2 Electronic structure calculations

The aim of computational physics, chemistry and materials science is to defined a many body system which could well be described by the many body Hamiltonian.

$$\hat{H} = \frac{-\hbar^2}{2m_e}\sum_i \nabla_i^2 - \sum_{i,I}^{N} \frac{Z_I e^2}{|r_i - R_I|} + \frac{1}{2}\sum_{i \neq j} \frac{e^2}{|r_i - r_j|}$$

$$- \sum_I \frac{^2}{2M_I}\nabla_I^2 + \frac{1}{2}\sum_{I \neq J} \frac{Z_I Z_J e^2}{|R_I - R_J|} \tag{3.1}$$

And simulating the physical properties of such systems is just solving the many-body Schroedinger equation of the systems. In many body electronic structure

calculations nuclei have much carrier than electrons, so we can consider motion of electrons separately from the nuclei. This method is called Born Oppenhamer Approximation (BOA).

3.2.1 Hartree-Fock approximation

Hartree-Fock method is a standard method of many particle theory first applied to atoms in 1930 by Fock [11]. In this method of approximation, for a fixed number of electrons N, an antisymmetrized by using slater determinant principle in which wave function can be formulated. This single wave function minimizes the total energy for the full interacting Hamiltonian (3.2)

$$\hat{H} = \hat{T} + V_{ext}(r) + V_{ee} \tag{3.2}$$

where T is kinetic energy, $V_{ext}(r)$ is external potential energy and Vee is Hartree energy.

But since this approximation fails to find the electron-electron interaction because this assumes that electrons are not interacting. This approximation says that $\hat{H}$ can be written as

$$\hat{H} = \sum^{N} h_(i) \tag{3.3}$$

where h is hamiltonian operator for i^{th} electron, $\hat{H}$ is the hamiltonian of all the system.

$$h_i \chi_j = \varepsilon_j \chi_j \tag{3.4}$$

where χ = eigen function of $\hat{h}$

Therefore,

$$\psi(\chi_1, \chi_2, \cdots \chi_n) = \chi_1 \chi_2 \cdots \chi_3 \tag{3.5}$$

In general the Hartree Fock (HF) method gives electron-electron repulsive interaction but not electron-electron correlation. The HF product doesn't satisfy the antisymmetric (change of position) the sign do not change on changing position. Exchange

interactions for the fermionic systems are not possible. HF relies on the following approximations:

- The Born-Oppenheimer approximation.
- The independent electron approximation [12].

3.2.2 Hartree-Fock Slater Determinant Method

In HFS approximation matrix type of multi Fermionic wave function is considered and this satisfy the antisymmetric. Each element of that matrix are single e^- orbitals. Rows of this matrix depend up on the number of electrons and column depends on position.

$$\psi = \frac{1}{(N!)^{\frac{1}{2}}} \begin{vmatrix} \chi_i(x_1) & \chi_j(x_1) & \cdots \chi_k(x_1)) \\ \chi_i(x_2) & \chi_j(x_2) & \cdots \chi_k(x_2)) \\ \vdots & \vdots & \cdots \quad \vdots \\ \chi_i(x_N) & \chi_j(x_N) & \cdots \chi_k(x_N)) \end{vmatrix} \tag{3.6}$$

The expectation value of Equation (3.2), with the wave function (3.5) is

$$\langle\phi|\hat{H}|\phi\rangle = \sum_{i,\sigma} \int dr \psi_i^{\sigma *}(r) \left[-\frac{1}{2} + V_{ext}(r)\right] + \frac{1}{2} \sum_{i,j,\sigma_i,\sigma_j} \int dr dr' \psi_i^{\sigma_i *}(r) \psi_j^{\sigma} *(r') \frac{1}{|r-r'|} \psi^{\sigma_j}(r')$$

$$-\frac{1}{2} \sum_{i,j,\gamma} \int dr dr' \psi_i^{\sigma *}(r) \psi_j^{\sigma *}(r') \frac{1}{|r-r'|} \psi_j^{\sigma}(r) \psi_i^{\sigma}(r') \tag{3.7}$$

3.2.3 The variational principle

In the HF wave function $\psi_i(r_i) = \sum_\mu \chi_\mu(r_i)$, that is the molecular orbital coefficients are determined using the variational theorem. The variational theorem says that, the energy determined from any approximate wavefunction will always be greater than the energy for the exact wavefunction.

The energy of the exact wave function serves as a lower bound on the

calculated energy and therefore the $C\mu_i$ can be simply adjusted until the total energy of the system is minimized [13].

3.3 Density Functinal Theory (DFT)

Density Functional Theory (DFT) is a succesfull theory to calculate the electronic structure of atoms, molecules and solids [14]. Its goal is for understanding of material properties from the fundamental laws of quantum mechanics [11, 14]. To address the limitations of traditional electronic structure method, a different approach is taken into density functional theory where instead of the many-body wave function, the one body density is used as the fundamental variable. Since the density $n(r)$ is a function of only three spatial coordinates (rather than the $3^N + N$ coordinates of the wave function). DFT is computationally feasible even for large systems.

The foundations of density functional theory are the Hohenberg-kohn and Kohn-Sham theorems.

3.3.1 Hohenberg-Kohn (HK) and Kohn-Sham Theorems

The central statement of formal density-functional theory is the celebrated HK theorems. In ground state DFT one is interested in systems of N interacting electrons described by the Hamiltonian [11]

$$\hat{H} = \hat{T} + \hat{V} + \hat{V}_{ee} = -\sum_{i=1}^{N} \frac{\nabla_i^2}{2} + \sum_{i=1}^{N} V(r_{i=1}) + \frac{1}{2}\sum_{i=1}^{N}\sum_{i=j=1}^{N} \frac{1}{|r_i - r_j|} \tag{3.8}$$

where, $\hat{H}$ is kinetic energy operator.

$\hat{V}$ is potential energy operator and

$\hat{V}_{ee}$ is interaction energy operator.

The Hohenberg–Kohn theorem provides the basic theoretical foundation

for the construction of an effective single-particle scheme which allows for the calculation of the ground-state density and energy of systems of interacting electrons. The resulting equations, the so-called Kohn–Sham equations, are at the heart of modern density-functional theory. They have the form of the single-particle Schrodinger equation.

$$\left[\frac{-\nabla^2}{2} + v_s(r)\right]\varphi_i(r) = \varepsilon_i\varphi(r) \tag{3.9}$$

The density can then be computed from the N single particle orbitals occupied in the ground-state slater determinant.

$$n(r) = \sum_{i}^{occ} |\varphi_i(r)|^2 \tag{3.10}$$

The central idea of the Kohn-Sham scheme is to construct the single particle potential v_s in such a way that the density of the auxiliary noninteracting system equals the density of the interacting system of interest. The Hohenberg-Kohn functional is

$$F[n](r) = T_s[n(r)] + U[n(r)] + E_{xc}[n(r)] \tag{3.11}$$

where T_s-is noninteracting kinetic energy.

$$U[n(r)] = \frac{1}{2}\int d^3r \int d^3r' \frac{n(r)n(r')}{|r - r'|} \tag{3.12}$$

is the classical electrostatic energy of the charge distribution $n(r)$, and $E_{xc}[n(r)]$ is the so called exchange correlation energy which is defined by

$$E_{xc}[n(r)] = T[n(r)] + V_{ee}[n(r)] - U[n(r)] - T_s[n(r)] \tag{3.13}$$

From the above definitions one can derive the form of the effective potential

$$v_s[n(r)] = v(r) + \int d^3r' \frac{n(r')}{|\mathbf{r} - \mathbf{r}'|} \tag{3.14}$$

where the exchange-correlation potential is defined by

$$v_{xc}[n(r)] = \frac{\partial E_{xc}[n(r)]}{\partial n(r)} \tag{3.15}$$

3.3.2 Approximations for the exchange correlation energy

While DFT itself does not give any hint on how to construct approximate E_{xc} functionals, it holds both the promise and the challenge that the true E_{xc} is a universal functional of the density, that is, it has the same functional form for all systems. On the one hand this is a promise because an approximate functional, once constructed, may be applied to any system of interest. On the other hand, this is a challenge because a good approximation should perform equally well for very different physical situations.

Local Density Approximation

Both the promise and the challenge are reflected by the fact that the simplest of all functionals, the so-called local density approximation (LDA), or its spin-dependent version, the local spin density approximation (LSD), has remained the approximation of choice for quite many years after the formulation of the Kohn–Sham theorem [14]. In LDA, the exchange–correlation energy is given by

$$E_{xc}^{LDA}[n] = \int d^3r n(r) e_{xc}^{unif}(n(r)) \tag{3.16}$$

where $e_{xc}^{unif}(n(r))$ is the exchange–correlation energy per particle of an electron gas with spatially uniform density n.

By its very construction, the LDA is expected to be a good approximation for spatially slowly varying densities. Although this condition is hardly ever met for real electronic systems, LDA has proved to be remarkably accurate for a wide variety of systems.

The Generalized Gradient Approximation

The only moderate accuracy that the local (spin) density approximation delivers is certainly insufficient for most applications in chemistry and other sciences [15, 16]. Hence, for the many years in which the LDA was the only approximation available for E_{xc}. The situation changed significantly in the early eighties when the first successful extensions to the purely local approximation were developed. The logical first step in that direcrtion was the suggestion of using not only the information about the density $n(r)$ at a particular point $\mathbf{r}$, but to supplement the density with information about the gradient of their charge density, $\nabla n(r)$ in order to account for the non-homogeneity of the true electron density [18, 19].

$$E_{xc}^{GGA} = \int n(r)\varepsilon_{xc}(n, \nabla_n)dr \tag{3.17}$$

In practice, E_{xc}^{GGA} is usually split into its exchange and correlation contributions

$$E_{xc}^{GGA} = E_{x}^{GGA} + E_{c}^{GGA} \tag{3.18}$$

and approximations for the two terms are sought individually.

3.3.3 Plane wave basis sets

In quantum chemistry and quantum physics, the basic parameters are the wavefunctions. In Gaussian wavefunctions, the Kohn-Sham Equation [equation 3.8] are a linear combinations of basis functions $\phi_i(r) = \sum_\alpha c_{i\alpha}\varphi_\alpha$, we required self-consistent solution and needed different basis sets for different molecules and solids. In addition, although this basis describes the atom very well, they are non-orthogonal, they depend on atomic positions, they have too many parameters. Therefore, for electronic structure calculations other convenient basis sets are required. These basis sets are plane-wave basis sets. Plane waves are orthogonal, independent of atomic positions, easy to use on any atomic type etc. In plane waves, we choose

the basis function as plane waves,

$$\varphi_\alpha(r) = \frac{1}{\sqrt{\Omega}} e^{i\overrightarrow{G_\alpha}.\overrightarrow{r}} \tag{3.19}$$

the suporposition of this plane-waves is:

$$\phi(\overrightarrow{r}) = \frac{1}{\sqrt{\Omega}} \sum_{\overrightarrow{G}} C_i(\overrightarrow{G}) e^{i\overrightarrow{G}.\overrightarrow{r}} \tag{3.20}$$

G is a vector of the reciprocall lattice. The reciprocal lattice vectors of the reciprocal lattice are:

$$b_1 = 2\pi \frac{a_2 \times a_3}{a_1.(a_2 \times a_3)} \tag{3.21}$$

$$b_2 = 2\pi \frac{a_3 \times a_1}{a_2.(a_3 \times a_1)} \tag{3.22}$$

$$b_3 = 2\pi \frac{a_1 \times a_2}{a_3.(a_1 \times a_2)} \tag{3.23}$$

3.3.4 Pseudopotentials

A present day electronic structure calculations, covering variety of topics relies on the pseudopotential framework [20, 21]. Pseudopotentials are used to include the core states of the material in the electronic structure calculations, there are more bands to solve and this needs much larger N_{PW}, for each band.

Norm-conserving Pseudopotential

The pseudopotential approach is based on the observation that most electronic properties of atoms are determined by the structure and dynamics of the atomic valence states [20]. On the other hand, these properties are affected only indirectly by the core electrons. The core electrons restricts the states available to the valence electrons in some binding or excitation processes through the orthogonality requirement.

There exists many types of pseudopotentials. In the DFT case, this usually

relies on the norm conserving pseudopotentials. Depending on the result of an all-electron DFT calculation for the atom of interest, the norm-conserving pseudopotential for angular momentum ℓ is choosen so that

(I) the resulting atomic valence pseudopotential orbital (PO) is identical with the corresponding atomic orbital (AO) for all $\mathbf{r}$ larger than some angular momentum dependent cutoff radius $r_{c,\ell}$

$$P^{ps}_{n\ell}(r) = P^{ae}_{n\ell}(r), \forall \;\; r \geqslant r_{c,\ell} \tag{3.24}$$

(II) the norm of the orbital is conserved

$$\int_0^{r_{c,\ell}} dr|P^{ps}_{n\ell}(r)|^2 = \int_0^{r_{c,\ell}} dr|P^{ae}_{n\ell}(r)|^2 \tag{3.25}$$

Ultrasoft Pseudopotential

Ultra soft pseudopotential (USPP) were introduced by Vanderbilt in 1990 [21] in order to allow calculations to be performed with the lowest possible cutoff energy for the plane-wave basis sets. In ultra soft pseudopotentials, the pseudopotential can be soft because norm conservation is not required. This gives it freedom to choose core radii. The principle behind ultra soft pseudopotential is that, in most cases, a high cutoff energy is only required for the plane-wave basis set when there are tightly bound orbitals that have a substantial fraction of their weight inside the core region of the atom. In these situations, the only way to reduce the basis set is to violate the norm-conservation condition by removing the charge associated with these orbitals from the core region. The pseudo wavefunctions are thus allowed to be as soft as possible within the core, yielding a dramatic reduction in the cutoff energy. Technically, this is accomplished by introducing a generalized orthonormality condition [21]. In order to recover the full electronic charge, the electron density given by the square moduli of the wavefunctions is augmented in the core regions. The electron density can thus be subdivided into

a soft part extending through the unit cell and a hard part localized in the core regions.

3.3.5 Electron phonon interaction

The superconducting properties of materials can be understood by calculating the electron-phonon interaction for a phonon mode, ν, with momentum $\mathbf{q}$ [22]. The electron-phonon coupling constant is:

$$\lambda_{q\nu} = \frac{\Delta\omega_q}{\pi\hbar N(e_F)\omega_q^2} \tag{3.26}$$

where $\Delta\omega_q$ is broadening (linewidth), N_{e_F} is DOS at Fermi level and ω_q is phonon frequency.

The electrons on the graphene π Fermi surface can couple only to in-plane optical carbon vibrations (C_{xy}) [22]. But this phonons give a small contribution due the factor $\frac{1}{\omega_q^2}$ in Equation 3.24, this factor supresses the weight of high energy optical phonons. This electron-phonon coupling constant (EPCC) is found using Equation 3.26. The electron-phonon mass enhancement parameter λ can also be defined as the reciprocal momentum of the phonon spectral function:

$$\lambda = \sum_{q\nu} \lambda_{qv} = 2\int \frac{\alpha^2 F(\omega)}{\omega} d\omega \tag{3.27}$$

To find the critical temprature T_c we have used the McMillan formula:

$$T_c = \frac{\omega_{log}}{1.2} exp\left[\frac{-1.04(1+\lambda)}{\lambda(1-0.62\times\mu*)-\mu*}\right] \tag{3.28}$$

where $\omega_{log} = exp\left[\frac{2}{\lambda}\int \frac{d\omega}{\omega}\alpha^2 F(\omega)\ln\omega\right]$, $\mu*$ is chemical coefficient.

3.4 Density Functional Perturbation Theory

Born and Hung (1954) are study lattice vibrations quantum mechanicaly and they found to describe dielectric phonons should be included [23]. But they didn't study the relations of these lattice vibrations with electronic motions. Connection between lattice vibration and electronic density of states (electron-phonon coupling) is first propose by Pic, Cohen and Martin. This theory is called linear response theory.

By using the linear response theory, Baroni (1987), Zain (1984) used this idea to develop codes of density functional perturbation theory (DFPT) [23]. They have used as input the Hohenberg-Kohn and Kohn-Sham theorems. This new theory gives phonon dispersion relation which can be fine grid of wave vectors.

Phonon frequency Calculations

Lattice dynamics is the second order change of the many body system with respect to the atomic positions. When the forces between lattices (ions) is zero, we call the model is fully relaxed. By changing the position of nuclei systematically the inter atomic forces become zero. that is:

$$F_I = \frac{\partial E(R)}{\partial R_I} = 0 \tag{3.29}$$

Therefore, first derivatives of energy over Born-Oppenhamer (BO) (model) gives structure relaxation. And second derivatives over Born-Oppenhamer (BO) surface gives lattice vibration frequency. That is:

$$\omega^2 = \frac{\partial F_I}{\partial R_I} = \frac{\partial^2 E(R)}{\partial R_I^2} \tag{3.30}$$

The computational algorithm which minimizes the inter-atomic forces work on the principle of systematic small displacement of atoms or molecules called as molecular dynamical algorithms. Newtonian algorith is one such algorithm which

minimizes the forces at each and every atom of given geometrical model. If we use pseudopotentials of lattice points for inter atomic force calculation, it is called quasi newton algorithm.

3.4.1 Helmann Feyman theorem

Since the dynamical matrix (Heisian matrix) for calculating the stable frequencies is difficult to get solutions. Hence to solve this problem Helmann and Fyman propose a technique known as Helmann-Fyman theorem. This theorem is an independent tool used in quantum mechanics for calculations of expectation values of the hamiltonian. That is:

$$\frac{\partial E_\lambda}{\partial \lambda} = \langle \psi_\lambda | \frac{\partial H_\lambda}{\partial \lambda} | \psi_\lambda \rangle \tag{3.31}$$

In our case the the parameter lambda is position and we are finding expectation values of energy.

3.4.2 Linear response theory

Linear response theorem describes the relation of electron density with lattice dynamics. The lattice pertubation induced changes in the ground state electron density brings the corrosponding changes in the energy eigenvalues by virtue of first order perturbation theory. Thus, the lattice dynamical perturbation induced effects are in the linear response of density with respect to nuclear geometry.

$$\frac{\partial^2 E_R}{\partial R_I \partial R_J} = -\frac{\partial F}{\partial R_J} = \int \frac{\partial n_R(r)}{\partial R_J} \frac{\partial V_R(r)}{\partial R_I} dr$$

$$+ \int n_R(r) \frac{\partial^2 V_R(r)}{\partial R_I \partial R_J} dr + \frac{\partial^2 E_N(R)}{\partial R_I \partial R_J} \tag{3.32}$$

That is evident from Equation 3.30, which says phonon vibration frequency is in linear response to density and from firs term of Equation 3.30, it is in linear response to $\frac{n_R}{R}$.

This theory is given by De Cicco (1969) [23] and it states that calculation of Hessian of BO energy surface is the the linear response to a disturbation (vibration) of nuclear geometry that is:

$$\frac{\partial n_R(r)}{\partial R} \tag{3.33}$$

This Hessian matrix is usually called as matrix of inter atomic force constants. Hence, in DFPT, the nuclei are perturbed (at different K values) and this results in their vibrations and linear response of density is calculated for respective perturbations.

Perturbation of the KS orbital i.e, $\Delta\psi_n(R)$ when used as eigen function for unperturbed KS hamiltonian H_{SCF} gives change in eigenvalues of KS orbital (ψ_n) in accordance with the first order perturbation theory, given by,

$$(H_{SCF} - \varepsilon_n)|\Delta\psi_n\rangle = (\Delta V_{scf} - \Delta\varepsilon)|\psi\rangle \tag{3.34}$$

The R.H.S. of above describes the application of KS orbital perturbations on the unperturbed Hamiltonian in ket-notations. While the quantities on the L.H.S. give corrosponding changes in the eigenvalues.

Chapter 4

Methodology

The results reported here were obtained from first-principles density functional theory in the generalized gradient approximation. The quantum espresso [17] software was used with norm-conserving pseudopotentials and a plane-wave cutoff energy of 816 eV. All of the structures considered were relaxed to their minimum energy configuration on the ATK software. Furthermore, we used quasi newton algorithm to model the graphene based structures. The monolayer systems were simulated in the dihedral angle of 0.000 degree in-plane unit cell Figure 5.1. Phonon frequencies were calculated using the linear-response technique on a phonon wave-vector mesh of 6 × 6 × 1 with a 12 × 12 × 1 uniform electron-momentum grid. 24 × 24 × 1 is used for band structure electronic density of states and phonon momentum mesh of 12 × 12 × 1 is used.

The Eliashberg function is :

$$\alpha^2 F(\omega) = \frac{1}{N(0)N_k N_q} \sum_{n,k,q} |g^{\nu}_{nk,mk+q}|^2 \times \delta(\varepsilon_{nk})\delta(\varepsilon_{mk+q})\delta(\omega - \omega^{\nu}_q) \tag{4.1}$$

where $N(0)$ is the total density of states, N_k and N_q the total numbers of k and q points respectively, n and m are band indices for the electron eigenvalues, ν is phonon frequency, $g_{nk,mk+q}$ represents the electron-phonon matrix element.

The total electron-phonon coupling $\lambda(\omega)$ is:

$$\lambda(\omega) = 2 \int \frac{\alpha^2 F(\omega')}{\omega} d\omega \tag{4.2}$$

The superconducting critical temperature was calculated using the McMillan formula with $\mu* = 0.115$.

4.1 Atomistix Tool Kit (ATK)

Atomistix Tool Kit (ATK) is a software package that offers unique capabilities for simulating electrical transport properties of nanodevices on the atomic scale. Based on an open architecture which integrates a powerful scripting language with a graphical user interface. ATK is a comprehensive platform for studies in nano-electronics, using methods that range from both accurate quantum-mechanical first-principles and fast semi-empirical methods to classical potentials for very fast geometry optimizations and molecular dynamics calculations. A special focus is placed on treating large-scale systems, with several thousand atoms. Moreover, ATK includes a very advanced electrostatic model to allow realistic simulations of nanoscale transistor structures. Virtual NanoLab (VNL) offers a rich set of powerful tools for investigating and analyzing the properties of nanostructures by simulating measurements by numerical calculations. It gives scientists, engineers, and researchers access to powerful atomic scale modeling tools. VNL provides convenient programs to

- design and build several types of nanostructures
- setup scripts for performing calculations
- inspect, analyze, and visualize your results.

Numerical calculations in VNL is processed by the "job manager", which combines advanced numerical methods, such as density-functional theory (DFT) and non-equilibrium Green's functions (NEGF), to describe the detailed electronic structure of nanoscale devices.

4.2 Quantum Espresso

QUANTUM ESPRESSO (open source package for research in electronic structure, simulation, and optimization) contains mainly

(1) Plane Wave self-consistent field

(2) CP (Car-Parinello) for the calculation of electronic structure properties within Density-Functional Theory [17].

4.2.1 Plane Wave self-consistent Calculations

Plane-wave self-consistent field of the Quantum Espresso package performs different types of "SCF" calculations of electronic and structural properties within DFT by using PW type basis set and norm-conserving pseudopotentials [17]. Using this package we can calculate:

• ground state energy and one-electron (Kohn-Sham) orbitals.

• atomic forces, stress and stress optimization.

• molecular dynamics on the ground state Born-Oppenhimer surface and other calculations [17]. In the PWscf SCF calculation, input data is organized by namelists. Following are some examples of namelists:

(I) &CONTROL: this namelist contains general variables controlling the scf calculation. In this namelist, there are several variables including

- **calculation**: this is a string describing the task to performed.
- **prefix**: this is to specify the input or output file name.
- **restart_mode**: this is used to perform the calculation.
- **tstress**: this is used to calculate the stress and so many other variables in the above namelist.

(II) &SYSTEM: this namelist is used for structural information on the system under investigation. In this namelist there are more than seventy variables. The main variables used for electronic and structural calculations are:

• **ibrav**: this variable uses to specify the lattice type of the material under investigation. In this variable, the lattice type (assigned from zero upto fourteen to the fourteen crystal structure) should be specified.

• **celldm()**: this variable describes the crstallographic constants of the material under investigation. These are:

celldm(1): is the lattice parameter 'a'.

celldm(2): is the lattice parameter 'b'.

celldm(3): is the lattice parameter 'c'.

• **ntyp**: this variable specifys the number of types of atoms in the supercell.

• **nbnd**: this describes the number of elecronic states (bands) to be calculated.

• **ecutwfc**: this calculates the kinetic energy cutoff **Ry** for wavefunctions.

(III) &ELECTRONS: this namelist controls the ectronic variables for self-consistency and smearing. In this namelist there are many namelists. To mention a few:

• **conv_thr** this variable uses for convergence treshold for self-consistency.

• **mixing_beta** this is a mixing factor for self-consistency.

• **mixing_mode** this variable describes the mode of charge density mixing.

There are also other several fields (cards) with self explanatory names including:

• &ATOMIC_SPECIES: with varibles like $X(1)$, $X(2)$, $mass\ X(1)$, $Pseudopot\ X(1)$ etc.

• &ATOMIC_POSITIONS: with variables $x(1)$, $y(1)$, $ifpos(1)(1)$, $ifpos(2)(1)$ etc.

• &K_POINTS: this card contains variables like $xk\_x(1)$, $xk\_y(1)$, $xk\_z(1)$ etc.

And there are other cards including cell parameter, constraints, and occupations.

4.2.2 Phonon calculations Using the Quantum Espresso

The codes available in the PHonon package of the main quantum espresso software can perform the following types of calculations [17]:

- phonon frequencies and eigen vectors at a generic wave vector, using Density-Functional Perturbation Theory;
- effective charges and dielectric tensors;
- electron-phonon interaction coefficients for metals;
- interatomic force constants in real space;
- third-order an harmonic phonon lifetimes;
- Infrared and Raman (non resonant) cross section.

The phonon package includes the following integrated codes and perform different activities:

- `PH/ph.x`: Calculates phonon frequencies effective charges and others (uses data produced by `pw.x`).
- `PH/dynmat.x`: applies various kinds of Acoustic Sum Rule (ASR), IR and Raman cross sections (if the coefficients have been properly calculated), from the dynamical matrix produced by `ph.x`
- `PH/q2r.x`: calculates Interatomic Force Constants (IFC) in real space from dynamical matrices produced by `ph.x` on a regular q-grid.
- `PH/matdyn.x`: produces phonon frequencies at a generic wave vector using the IFC file calculated by `q2r.x`; may also calculate phonon DOS, the electron-phonon coefficient λ, the function $\alpha^2F(\omega)$
- `PH/lambda.x`: also calculates λ and $\alpha^2F(\omega)$. plus T_c for superconductivity [17] and other codes.

4.2.3 Electronic structure calculations

To calculate the electronic structure of graphene and other materials self consistentently there are different codes (scripts), the following script is a general example.

&control

calculation='scf' this calculates the self consistency.

restart_mode='$from\_scratch$', is used to continue an interrupted calculation.

prefix='gr' is used to prepended to input/output file names.

tstress = .true. is used calculate stress. It is set to TRUE. if calculation = 'vc-relax'.

tprnfor = .true. is used to print forces. Set to .TRUE. if calculation =' relax'.

pseudo_dir = './', is a directory containing pseudopotential files.

outdir='./ is the place to put temporary output files.

/

&system

ibrav = 4, is the braviace lattice index.

celldm(1) = 8.055,the firs lattice parameter.

celldm(3) = 20, the second (y-axis) lattice parameter.

nat = 6, the number of atoms in the material.

ntyp = 1, the number of types of atoms in the system.

ecutwfc = 50, optimized energy cutoff.

/

&electrons

conv_thr = $1.0d^{-12}$ is the convergence threshold for self consistency.

mixing_beta = 0.7 mixing factor for self-consistency.

mixing_mode = 'plain' is use for charge density Broyden mixing.

/

ATOMIC_ SPECIES

C 12.0107 C.pbe-mt_fhi.UPF pseudopotential adress of carbon atom.

K_POINTS (automatic)

6 6 6 1 1 1 the brillouin zone points.

Each of these input parameters have meanings that need to be considered. Any of the sections that have an ampersand are name list or "cards" and the rest

are simple parameter specifications or fields.

In this software package we first perform a SCF calculation; then do a non-SCF calculation with the desired k-point grid and number of bands (nbnd). Specify instead calculation = 'nscf' if we are interested in further processing of the results of non-SCF calculations (for instance, in DOS calculations). In the later case, we should specify a uniform grid of points. For DOS calculations we should choose occupations = 'tetrahedra', together with an automatically generated uniform k-point grid (card K POINTS with option "automatic"). Variables prefix and outdir, which determine the names of input or output files, should be the same in the two runs (scf and nscf).

4.2.4 ENTOTO Computing Center

ENTOTO Computing Center is a supercomputing center owned by Chemistry Dept ,Addis Ababa University. Basically, it is a linux (Centos) based parallel cluster computation facility that comprises of 11 nodes, out of which one serves as the server working on the torque toolbox for complete parallization. Each node has the capability of 48 parallel processing and 10 nodes are reserved for the central server tasks. Hence, at any time 518 processors are available for parallel computation of open source Portable Batch System (PBS) type. Our computation directory is **tgroup4@10.4.17.30** that stores all the graphene related electronic and phonon calculations. With 22 TB storage, we can keep record of these calculations for the future referencing work.

Chapter 5

Results and discusion

In this work we have optimized the structural properties of pristine graphene, potassium doped graphene and rubidium doped graphene structures. We have used first principles density functional theory and the quantum espresso software for this purpose. In this chapter, we performed mainly three things: 1) Structural optimization of pristine graphene, potassium doped graphene and rubidium doped graphene 2) electronic structure calculations of pristine graphene, potassium doped graphene and rubidium doped graphene 3) phonon calculations of pristine graphene, potassium doped graphene and rubidium doped graphene. The adsorption geometry is obtained from the positions of the atoms after relaxation. The adatom heights have been taken 2.815 $\mathring{A}$ and 2.938 $\mathring{A}$ for potassium doped graphene and rubidium doped graphene, respectively.

5.1 Parameter optimization of graphene

Using the quantum espresso scripter, we prepared a script to generate the optimized structure of pure graphene. The C-C bonds are found to be 1.4186 $\mathring{A}$ which are smaller than the C-C bond lengths of diamond of 1.52 Å. This optimized graphene structure is shown in Figure 5.1. It is well-known that each carbon atom in the graphene hexagon has two 2s and two 2p electrons in its valence state. These four electrons lead to various sp-hybridized orbitals.

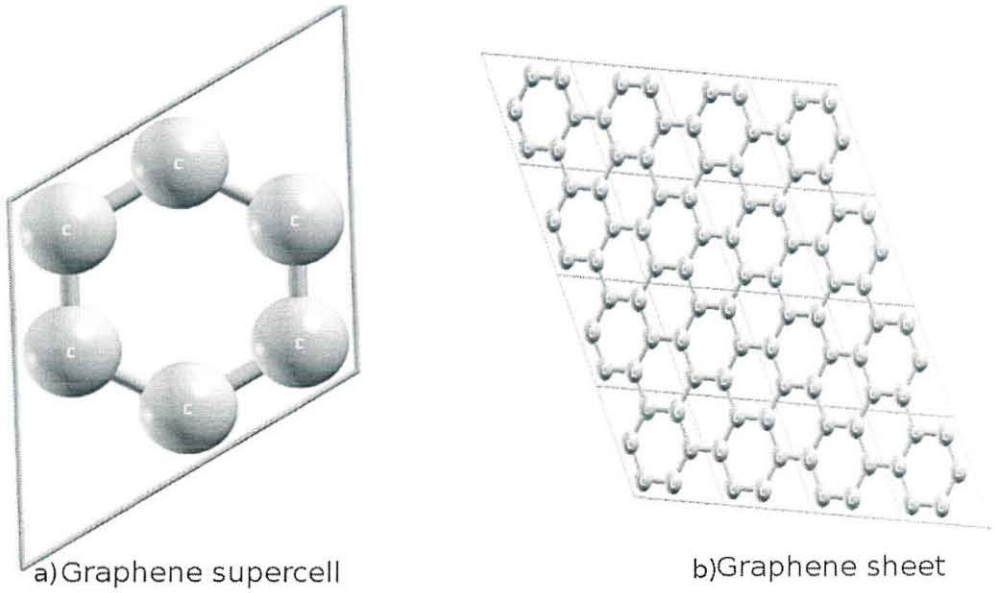

Figure 5.1: *Optimized pure graphene, a) graphene supercell and b) graphene sheet*

For graphene, each carbon atom is bonded to three other carbon atoms according to an sp^2 hybridization. We have used the quasi-Newton algorithms for our optimizations. The Quasi-Newton algorithm is used for finding extreme values. Quasi-Newton methods are based on Newton's method to find the stationary point of function, where the gradient is zero. In Newton's method the function is approximated as quadratic around the optimum. First and second derivatives of energies with respect to position is used to find the stationary point [26].

5.1.1 Lattice constant optimization

The lattice parameter of pristine graphene is optimized by first principles density functional theory using the quantum espresso software. The generalized gradient approximation (GGA) and norm-conserving pseudopotential are used to get the equilibrium lattice parameter. Equilibrium lattice constant of the pristine graphene is optimized by fixing the energy cutoff to 816 eV. We vary input files for 3.837895 $\mathring{A}$, 3.890795 $\mathring{A}$, 3.943695 $\mathring{A}$, 3.996595 $\mathring{A}$, 4.049495 $\mathring{A}$, 4.102395 $\mathring{A}$, 4.155295 $\mathring{A}$, 4.208195 $\mathring{A}$, 4.261095 $\mathring{A}$, 4.313995 $\mathring{A}$, 4.366895 $\mathring{A}$, 4.419795 $\mathring{A}$, 4.472695 $\mathring{A}$, 4.525595 $\mathring{A}$, 4.578495 $\mathring{A}$, 4.631395 $\mathring{A}$, 4.684295 $\mathring{A}$, 4.737195 $\mathring{A}$.

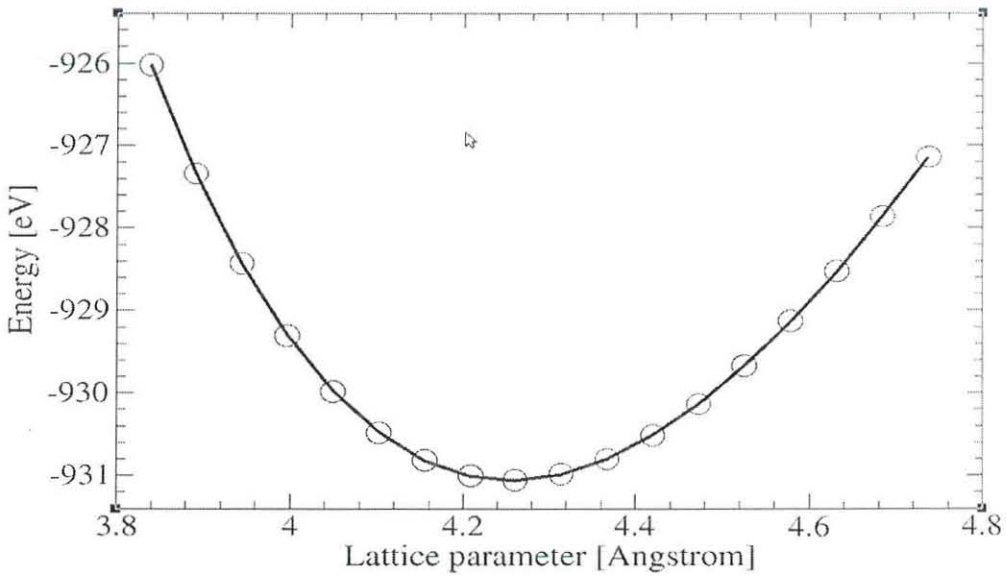

Figure 5.2: *The lattice constant optimization for pristine graphene*

Figure 5.2 shows the lattice constant optimization of graphene supercell. We have used the quasi newton technique to do the optimization. As we can see from Figure 5.2, it is symmetrical at the lattice constant **4.2610 Å**. Therefore we have choosen this lattice parameter for our further electronic structure calculations.

5.1.2 Energy cutoff mesh and k-points optimizatiom

Our calculations are performed within the first-principles DFT under the generalized gradient approximation (GGA) of Perdew, Burke, and Ernzerhof (PBE). The quantum espresso software is used to perform this calculations. A plane-wave basis set with a maximum plane-wave energy of 816 eV is used for the valence electron wave functions.

To find the energy cutoff, we have prepared a script containing energy cutoff values: 68, 136, 204, 272, 340, 408, 476, 544, 612, 680, 748, 816, 884, 952, 1020, 1088, 1156, 1224,1292, 1360 eVs. and the energy cutoff starts to be smooth starting from 816 eV and above as shown in Figure 5.3. Therefore, we can take the cutoff energy for pristine graphene 816 eV.

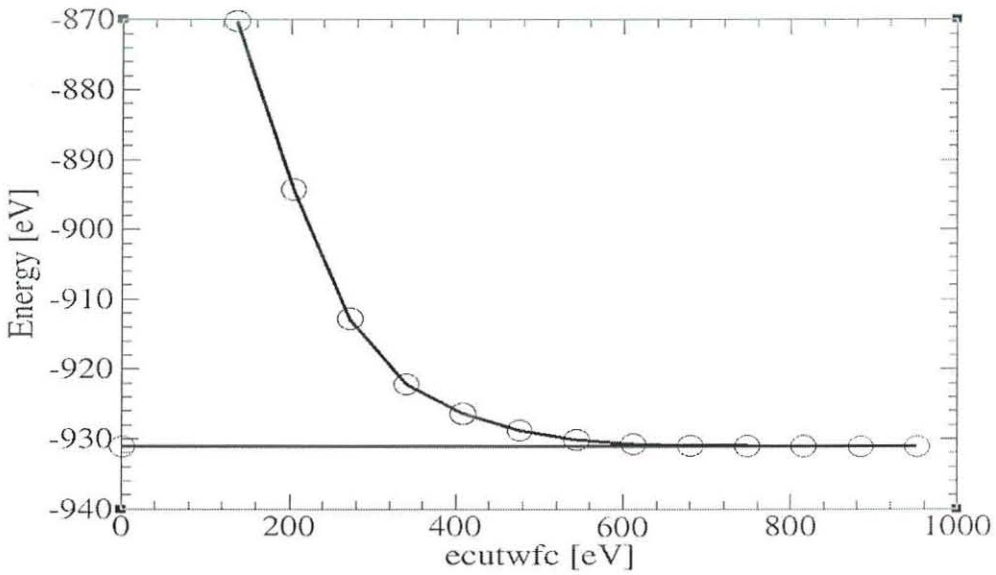

Figure 5.3: *The ecutwfc optimization for pristine graphene. The energy is smooth from about* 816 eV − 1088 eV

We optimized the k-points for the pure graphene. Figure 5.4 shows the k-point versus energy graph. If we observe the the graph, it turns at the k-points of $5 \times 5 \times 1$ but it starts to be smooth at the k-points of $6 \times 6 \times 6$. Therefore we take the K-points to be $6 \times 6 \times 6$ of course since graphene is two dimensional, we can take also $6 \times 6 \times 1$ (there is no z-axis). Taking higher K-point values give more accurate results, but it is expensive computationally.

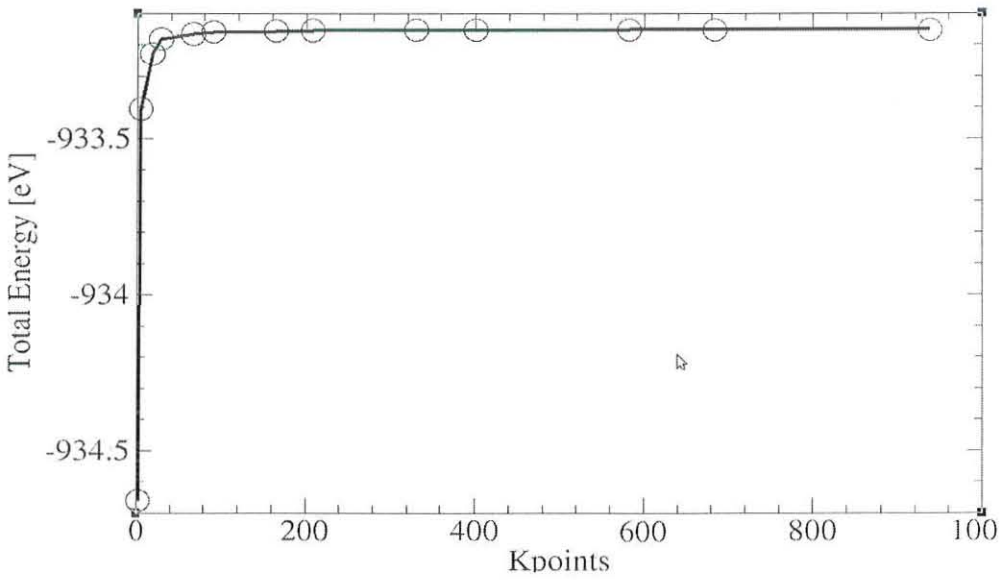

Figure 5.4: *The K points optimization for pristine graphene*

5.2 Preparation of rubidium-doped graphene

Rubidium is a 16^{th} abundant element of the periodic table. It has similar properties with the other alkali elements of the periodic table. Since all alkali metals are expected to induce superconductivity on doping on graphene surface, we have expectations that doping graphene with rubidium atom at the hollow site of the graphene sheet at an optimized height also brings superconductivity.

Similar to the pristine graphene, we optimized the *Rb*-doped graphene. We fixed the *Rb* atom, that is we constrained the *Rb* atom and the carbon atoms rearrange themselves to their equilibrium positions. The doping site for rubidium atom is the hollow site (**H**). We have created graphene supercell with a hexagonal *C* atoms and doped with *Rb* atom at the center of graphene supercell. The height of the graphane-adatom is also optimized to 2.9388 $\mathring{A}$. The optimized structure of *Rb*-doped graphene looks like Figure 5.5. In this figure a) shows the rubidium-doped graphene supercell and b) shows rubidium-doped graphene sheet. The angle between carbon atoms is 120.001 degrees and the dihedral angle is 67.221 degrees. This rubidium atom is responsible for the increament in density of states and bring superconductivity.

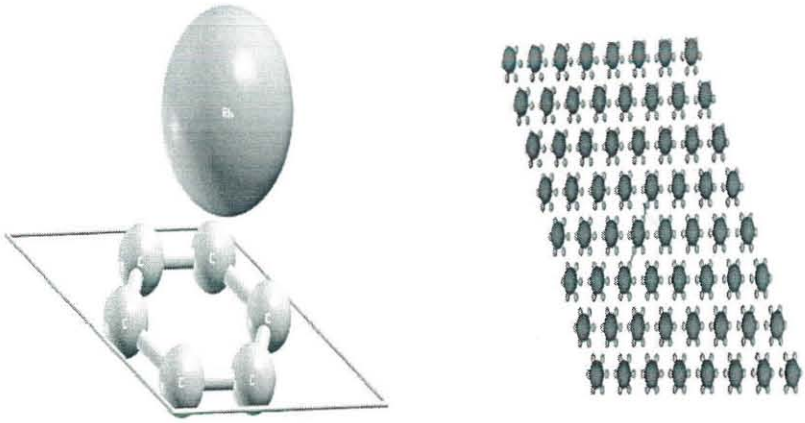

a) Rb-doped supercell b)Rb-doped sheet

Figure 5.5: *optimized Rubidium-doped graphen a) graphene supercell and b) graphene sheet*

5.2.1 Lattice constant optimization of Rb-doped graphene

Using first principles of density functional theory and the quantum espresso software, PWscf package, we optimized the lattice parameters of rubidium-doped graphene. To do this, we fixed the values of ecutwfc and K-points. We chose ecutwfc = 816 eV and k-points = 6. We assembled the results of SCF calculations for the dependence of total energy on lattice constant in a data file, e.g., we called etotvsalat.dat (this is plotable data type). To obtain optimized values of lattice parameters of rubidium-doped graphene, we prepared a script for different values of lattice parameters. These parameters are: 3.837895, 3.890795, 3.943695, 3.996595, 4.049495, 4.102395, 4.155295, 4.208195, 4.261095, 4.313995, 4.366895, 4.419795, 4.472695, 4.525595, 4.578495, 4.63139, 4.684295, 4.737195 $\mathring{A}$. And we have found a minimum energy of -944 eV at a lattice constant of 4.273791$\mathring{A}$. If we observe Figure 5.6 carefully and compare it with the pure graphene lattice parameters (Figure 5.2), the lattice parameter of rubidium-doped graphene is a little bit larger than the pristine graphene one. The energy is symmetric about the minimum value of the lattice parameter.

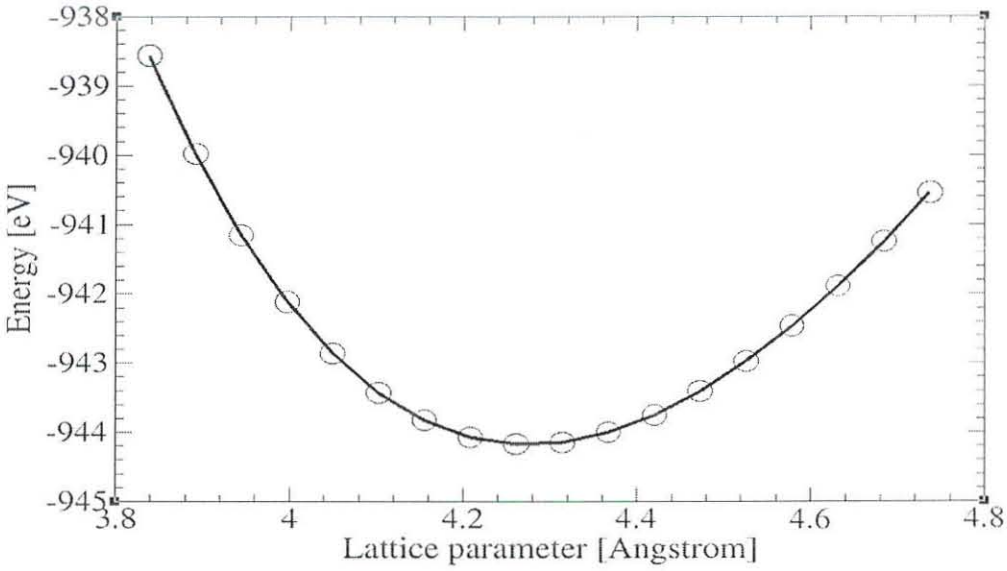

Figure 5.6: *The lattice constants of rubidium doped graphene*

5.3 Preparation of Potassium-doped graphene

Since graphene is single layer of graphite, this material becomes superconducting after intercalation with alkali or alkaline-earth metals [27]. These graphite intercalation compounds (GICs) can be viewed as a set of doped graphene layers in which the superconductivity originates in graphene sheets while the main role of the intercalants is to provide the charge to fill the graphene π^* states.

We expect that potassium doping would be an efficient technique for modifying the electronic structure in graphene to bring out superconductivity. Recent reports show that it is possible to dope K into SLG by the vapor transport method, and control of the electronic structure of SLG have also been demonstrated [27].

As we have done for the Rubidium-doped graphene, for the K-doped graphene also we optimized using the quasi-newton algorithm. We have created graphene sheeet with a hexagonal C atoms and doped with K atom at the center of graphene sheet. The height of the potassium atom from the graphene sheet is also optimized to the value of $\mathbf{h} = 2.81509$Å). The geometry of the Potassium-doped graphene is shown in Figure 5.7. The dehideral angle between the graphene sheet and the potassium atom is 66.283 degrees.

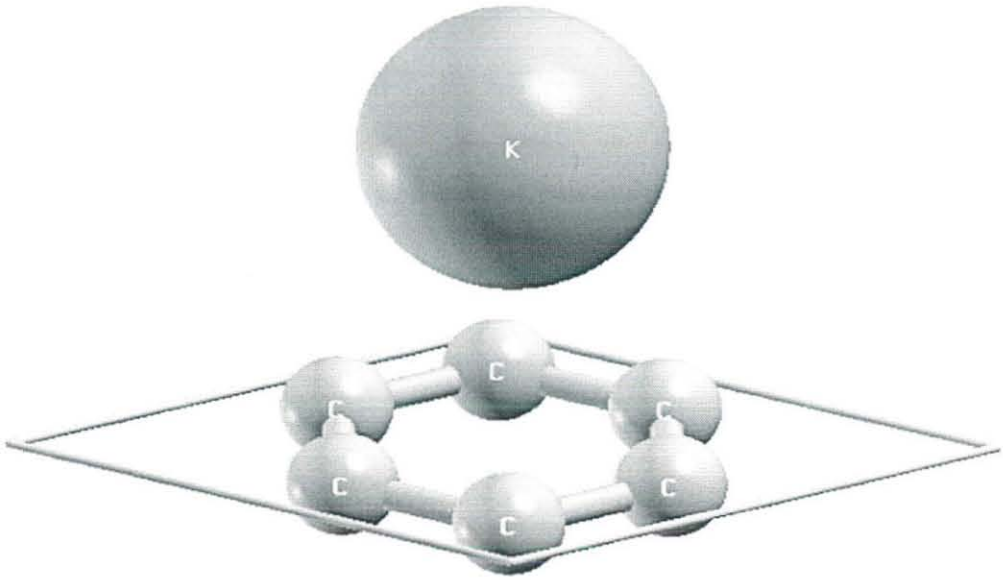

Figure 5.7: *optimized K-doped graphen*

The potassium atom makes an angle of 26.147 degrees with each carbon atom.

5.3.1 Lattice constant optimization of K-doped graphene

Potassium makes an ionic bonding when adsorbed by graphene sheet. In this simulation, the quantum espresso, PWscf package is used to perform optimization. A plane wave basis sets with a gaussian smearing of 0.01058 eV is used for the occupation of the electronic levels.

Similar to the rubidium-doped graphene case, in the K-doped graphene, we fixed the values of ecutwfc and k-points. We chose the energy cutoff (ecutwfc) = 816 eV and k-points = 6. We assembled the results of potassium-doped graphene SCF calculations for the dependence of total energy on lattice constant. To obtain optimized values of lattice parameters of potassium-doped graphene, we prepare a script for different values. For K-doped graphene, we have also calculated the energies for the following values of lattice constants:3.83789, 3.89079, 3.94369, 3.99659, 4.04949, 4.10239, 4.15529, 4.20819, 4.26109, 4.31399, 4.36689, 4.41979, 4.47269, 4.52559, 4.57849, 4.63139, 4.68429, 4.73719 $\mathring{A}$s. And at the lattice

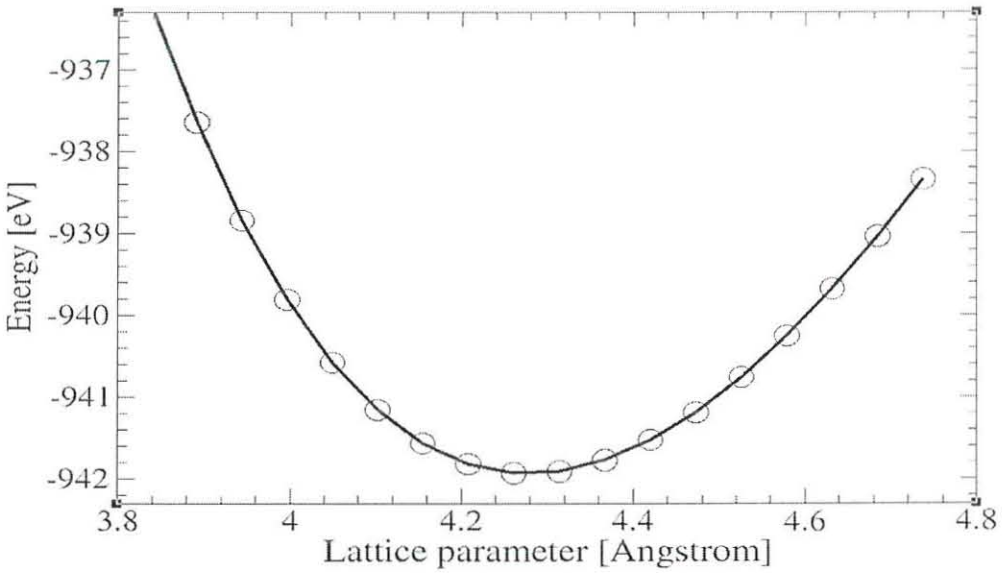

Figure 5.8: *results of lattice parameter optimization of K-doped graphen*

constant 4.282784 $\mathring{A}$, the minimum energy is $-942.2\ eV$. Figure 5.8 shows our result of lattice parameters optimization of K-doped graphene. At ≈ 8.1 the graph changes symmetricaly. If we compare this Figure 5.8 with the pristine graphene lattice parameters Figure 5.2, the lattice parameter increases from 4.25845 $\mathring{A}$ to 4.2849 $\mathring{A}$.

5.4 Electronic band structure calculations for pure graphene

It is rather important for our present comparative study to start with the structural and electronic properties of the pristine graphene. It is well-known that each carbon atom has two 2s and two 2p electrons in its valence state. These four electrons lead to various sp-hybridized orbitals. For graphene, each carbon atom is bonded to three other carbon atoms according to an sp^2 hybridization. In the present calculations the C-C bonds are found to be $1.41\mathring{A}$ which are smaller than the C-C bond lengths of diamond of $1.52\mathring{A}$. The C-C-C angle is measured to be 120 degrees, which is slightly larger than the prospective value of 109.5

degrees in its diamond structure. These values suggest that, unlike the ideal sp^3 diamond structural phase, graphene has a significant sp^2 nature as stated above. This feature, therefore, leads to the considerable rigidity of graphene materials comparing with the normal semiconducting materials. The electronic band structure and density of states(DOS) of pure graphene sheet is plotted in Figure 5.9 along the principal directions of the hexagonal Brillouin zone. It is clearly shown that the band structure of pristine graphene has a zero-gap semiconducting nature. It is important to note that the folding of the bands in the quantum espresso software. In this plot, the top of the valence state and the bottom of the conduction state degenerate at the Γ point (Dirac point) instead of the k-point of the hexagonal Brillouin zone. These two bands obey a linear in-plane dispersion relation near the Fermi energy at the Γ point of the Brillouin zone resulting in zero effective mass for electrons and holes and high mobility of charge carriers. As we can see from the Figure, the density of states (DOS) is almost zero at the Fermi level.

Graphene has two atoms per unit cell, which results a conical points of the Brillouin zone. Near these points the electron energy is linearly dependent on the wave vector [24]. The fact that charge carriers in graphene are described by the Dirac-like spectrum, rather than the usual Schrodinger equation for nonrelativistic quantum particles, can be seen as a consequence of graphene's crystal structure, which consists of two equivalent carbon sub-lattices. Quantum mechanical hopping between the sublattices leads to the formation of two energy bands, and their intersection near the edges of the Brillouin zone yields the conical energy spectrum. As a result, quasiparticles in graphene exhibit a linear dispersion relation $E = \hbar\kappa v_F$, as if they were massless relativistic particles (for example, photons) but the role of the speed of light is played here by the Fermi velocity $v_F = \frac{c}{300}$. Due to the linear spectrum, one can expect that graphene's quasiparticles behave differently from those in conventional metals and semiconductors where the energy spectrum can be approximated by a parabolic (free-electron-like) dispersion relation.

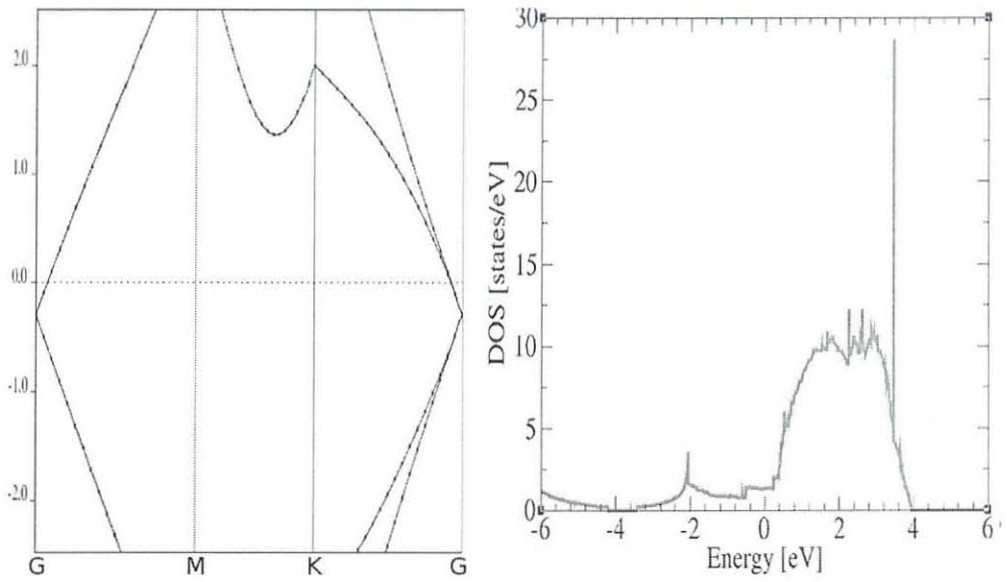

Figure 5.9: *Electronic density of states and band structure of pure graphene*

5.5 Electronic structure calculations of rubidium-doped graphene

Rubidium is discovered by the German chemists Robert Bunsen and Gustav Kirchhoff in 1861. Rubidium is a soft, silvery-white metallic element of the alkali metals group and it is one of the most electropositive alkali elements. Rubidium is the 16^{th} most abundant element in the earth's crust and it does not have any treat to environment.

In electronic structure calculations of rubidium-doped graphene, it is similar to the graphite intercalation compounds (GICs), the charge transfer from the intercalant atoms to the graphene sheets, resulting from the occupation of the π^* bands [28], we find that an interlayer state, which is well-separated from the carbon sheets, also becomes occupied. We show that the energy of the interlayer band is controlled by a combination of its occupancy and the separation between the carbon layers [29]. The graphene-alkali atom (rubidium in this case) should be at an optimal height since large and too small intercalant–graphene layer distance could also be deterimental for superconductivity [1].

We prepared Rb-doped graphene using the quantum espresso softwares PWscf package. The rubidium-doped graphene script has three name lists with different variables and three fields. We have set calculation = 'bands' in the first name list (control). In the second name list (system), we set the number of bands (nbnd) to 28. In the first field (ATOMIC SPECIES), we put the adress of pseudopotentials of the carbon atom and rubidium atom. In the second field (ATOMIC POSITIONS), we placed the coordinate positions of the six carbon atoms and one rubidium atom. And in the third field (K-POINTS), we have set the 61 k-points.

The core-valence interaction is obtained by norm-conserving pseudopotentials. We have taken plane-wave cutoff energy of 816 eV. Our structures were taken to their minimum energy configurations (as we discused in sections 5.1 and 5.2 above). The Fermi energy for heavy metals doping is displaced in to the graphene conduction π^* band [31]. So the Fermi energy for *Rb*-doped graphene is calculated to $E_F = -2.6867\ eV$ while our undoped supercell was $-3.517\ eV$. Figure 5.10 shows the band structure of our *Rb*-doped graphene. The density of states of *Rb*-doped graphene Figure 5.10 increases compared to our undoped (pristine graphene).

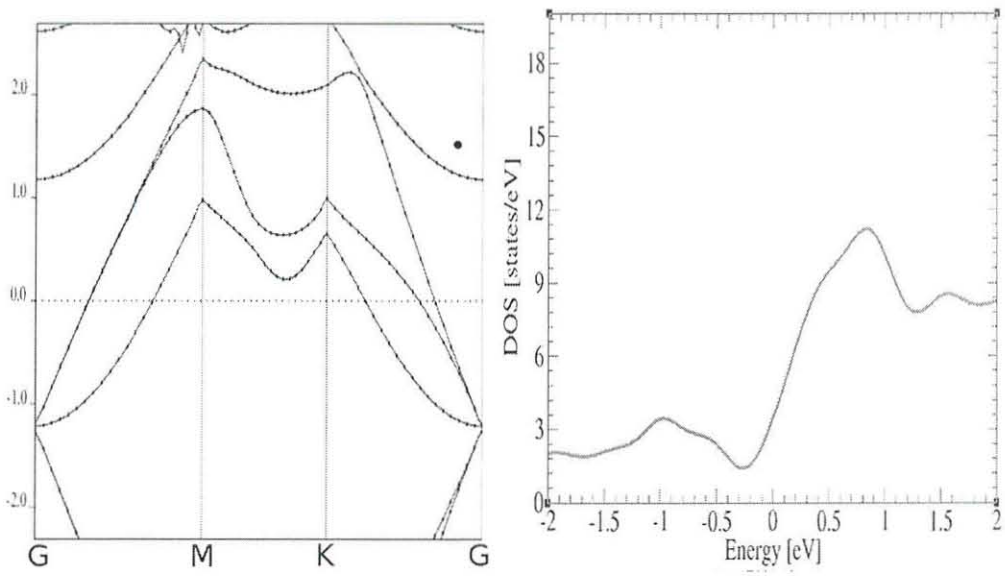

Figure 5.10: *Band structure and density of states for Rb-doped graphen for energy values from 2 eV to −2 eV*

5.6 Electronic structure calculations of potassium-doped graphene

In this part, we focus on the electronic energy bands and density of states of potassium-doped graphene which correspond to a doped graphene monolayer. We provide extensive theoretical evidence for this claim employing a theoretical approach using density-functional theory and including exchange correlation energies.

The adsorption of K on graphene leading to ionic bonding [29]. In this simulation, the quantum espresso package is used to perform calculations. A plane wave basis set with a maximum energy of 816 eV is used. A Gaussian smearing with a width of 0.01058 eV is used for the occupation of the electronic level. $6 \times 6 \times 6$ K-points has been used. The calculated equilibrium lattice parameter is 4.283 eV. The distance between two adjacent graphene layers is fixed 1.4276 eV. The Fermi energy is larger for K-doped graphene than pure graphene. Because there are more number of electrons in the K-doped graphene.

Omar Faye (et al [29]) explained for the K-doped graphene and showed an increament of electrons in doped graphene than the pristine one.

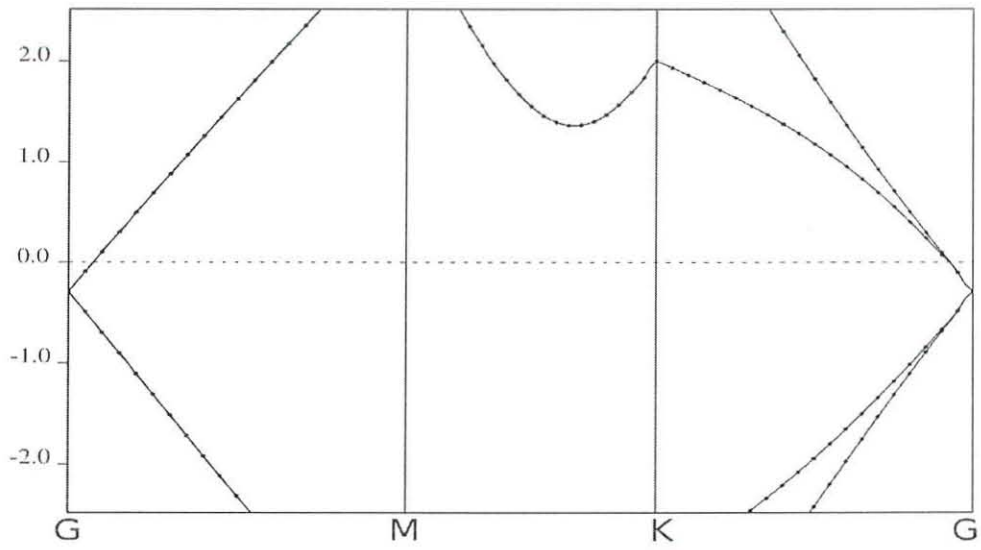

Figure 5.11: *Band structure of K-doped graphen for energy values from 2 eV to −2 eV*

In Figure 5.12, the band structure of potassium-doped graphene calculated within DFT is compared to the band structure of the electrostatic undoped graphene. The comparison reveals that the band structure changes close to the Dirac point due to deeper band coming from K atom. We calculate the Kohn-Sham band structure within the generalized gradient approximation (GGA) of density functional theory (DFT). 28 bands are are considered in the script of the potassium-doped graphene in plane waves with an energy cutoff at 816 eV. Core electrons are accounted for by norm-conserving pseudopotentials.

5.7 Phonon band structure calculations for pristine graphene

Phonon in graphene have been studied by density functional theory calculations [32, 33]. Calculations are performed within the generalized gradient approximation (GGA), using the density functional perturbation theory (DFPT) scheme, which allows the exact (within DFT) computation of phonon frequencies at any Brillouin Zone (BZ) point. We use plane-waves (816 eV cut-off) and norm-conserving

pseudopotentials approaches. We treat the semi-metallic character of the system by performing the electronic integration with a smearing technique, i.e. occupying the electronic levels according to a distribution with a finite fictitious electronic temperature $\sigma = 0.02645\ eV$.

The phonon dispersion branches are: an out-of-plane acoustic mode (**ZA**), an in-plane transverse mode (TA), an in-plane longitidunal (LA), an out-of-plane optical mode (ZO), an in-plane transverse mode (TO) and in-plane longitidunal optical mode (LO).

Three of the above six branches, these are, the out-of-plane acoustic mode (ZA), in-plane transverse acoustic mode (TA) and in-plane longitidunal acoustic mode (LA) are originated from the Γ-point of the brillouin zone in an increasing energy order [34].

The graphene phonon dispersions are shown in Figure 5.12, where phonon energy is ploted along high symmetry lines in the hexagonal Brillouin zone. Near the Γ-point (q = 0), there are three acoustic and three optical branches. As we can see from Figure 5.12, the lowest acoustic branch is an out-of-plane transverse mode (ZA) whose energy varies as q^2. The other two in-plane acoustic modes energy varies linearly as $|q|$. The lower of these three modes is the transverse acoustic mode (TA). And the higher is a longitudinal acoustic mode (LA). The lowest lying optical branch is an out-of-plane transverse mode (ZO) with a negative q^2 energy dependence at the Γ-point. The remaining two optical branches are in-plane transverse (TO) and longitudinal optical (LO) modes which have equal energy at the Γ-point (degenerate). The density of states for phonon modes in units of "modes per hexagonal unit cell per eV" is shown in Figure 5.13.

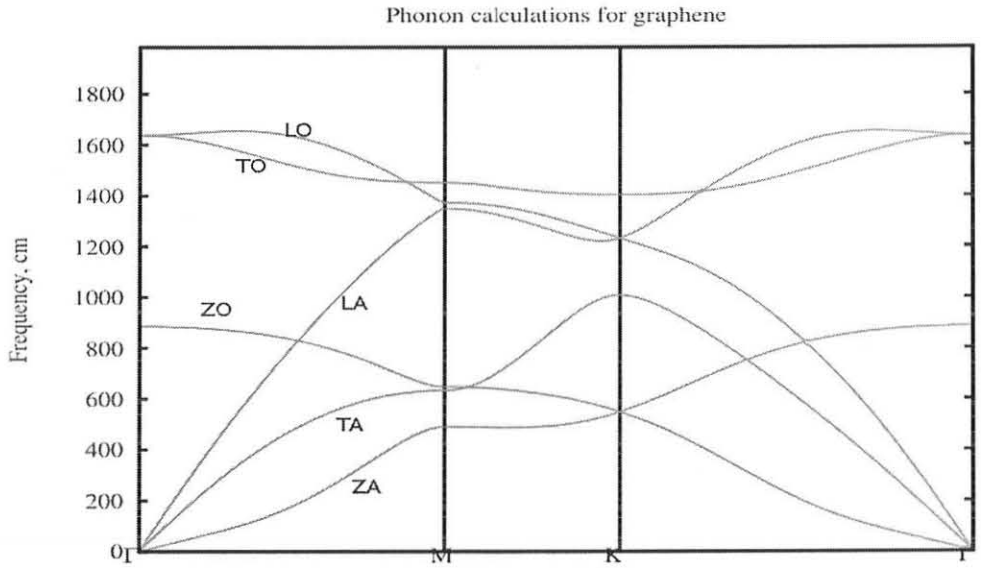

Figure 5.12: *phonon dispersion relation of pure graphene*

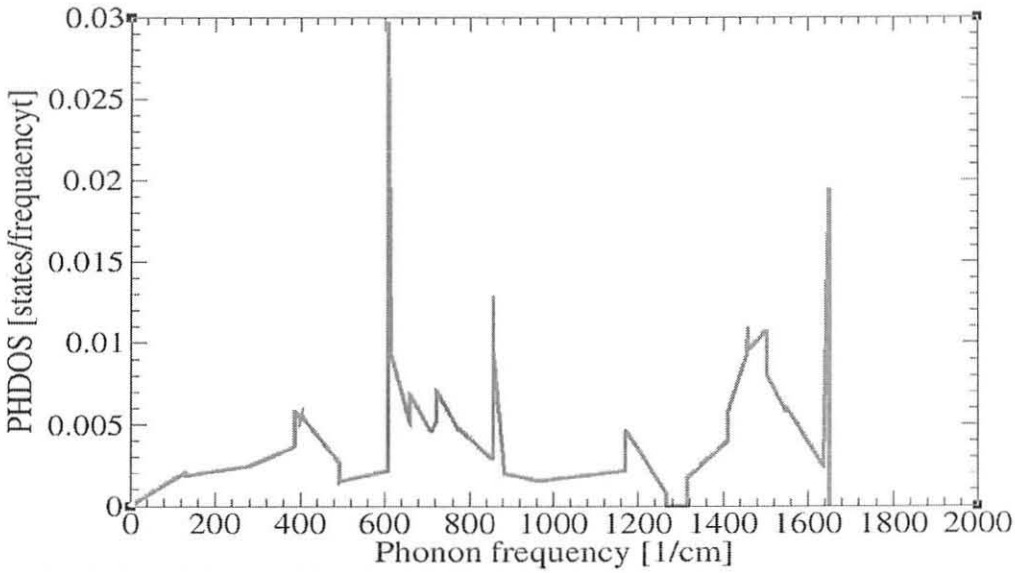

Figure 5.13: *Phonon density of states for pristine graphene*

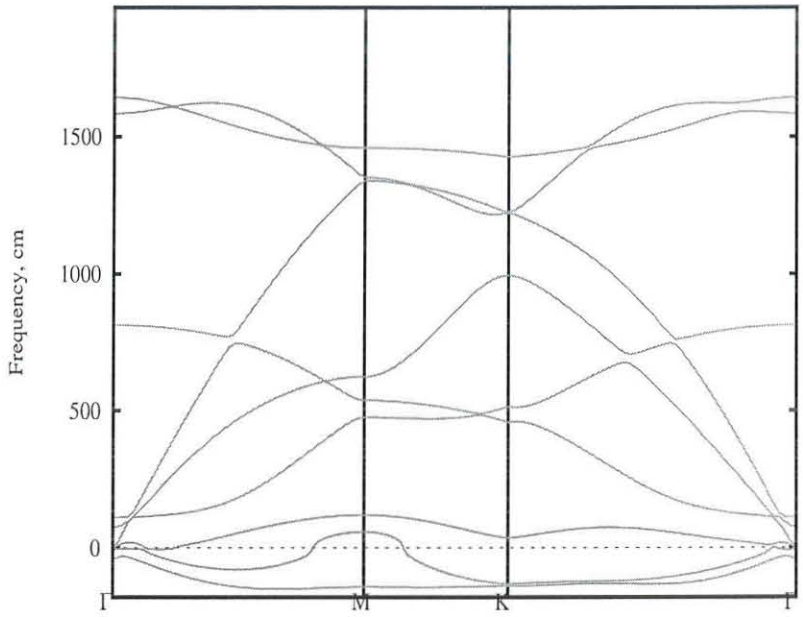

Figure 5.14: *Phonon band structure for Rb-doped graphene*

5.8 Phonon dispersion relations for rubidium-doped graphene

The relative position of the HOMO and LUMO of the adsorbate with respect to Dirac point in rubidium-doped graphene determines the direction of charge transfer. The Brillouin zone was sampled with a grid of $6 \times 6 \times 1$ K-points within the Monkhorst-Pack scheme.

The interaction between electrons and phonons in graphene and graphite has been studied with many experimental techniques including inelastic X-ray scattering (IXS), Scanning Tunneling Spectroscopy (STS), and Raman Spectroscopy [35]. In the rubidium-doped graphene the number of phonon dispersions is increased from the pristine graphene (Figure 5.14). The increament of phonon peaks is near to the Fermi level and this indicates that this material could be a superconductor. The optical phonon mode with frequency 120 cm^{-1} is in the good range for coupling with electrons. Graphene based devices is governed by electron-phonon coupling (EPC) or by deformation potential.

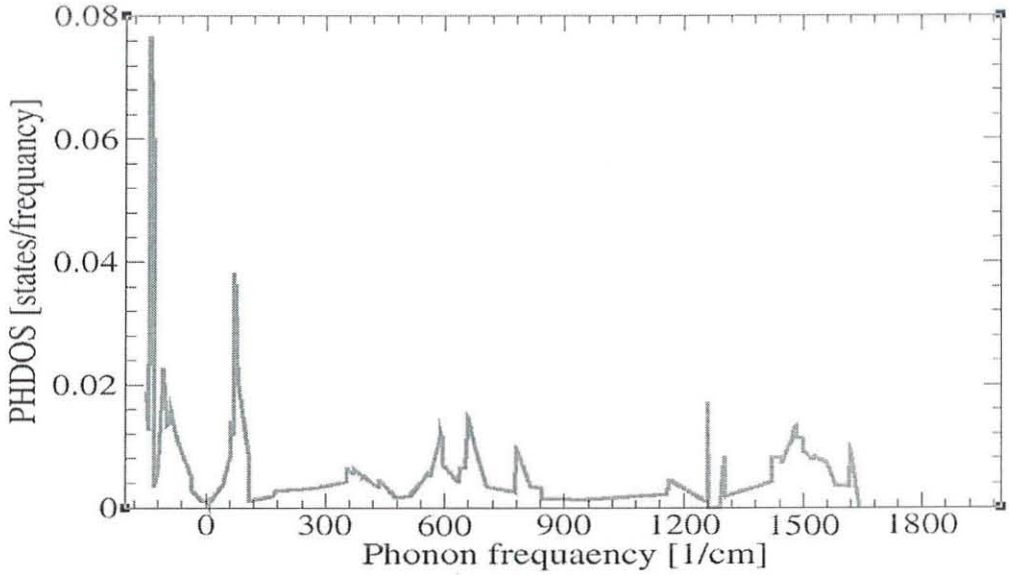

Figure 5.15: *Phonon density of states for Rb-doped graphene*

The deformation potential displays a strong doping dependence which would be taken into acount in the design of new graphene structures. For instance our Rb-doped and K-doped graphene structures. If we look Figure 5.15, we observed there is very high peak at around 120 cm^{-1}, the highest coupling constant is at similar phonon frequency. This shows us there is good agreement in phonon frequency and phonon density of stattes (PHDOS) around the Fermi level. Because the Fermi level for rubidium-doped graphene lowers/shifts from the pristine one.

5.9 Phonon dispersion relations for potassium-doped graphene

In graphite intercalation compounds (GICs), superconductivity was observed with transition temprature, T_c, ranging from below 1 K for alkali-metal adatoms [e.g: 0.5 K for KC_8 upto 11.5 K for CaC_6] [36]. This properties of GICs attracts into the electronic properties of doped few layer graphene (FLG). Intercalation of adatoms leads to shift in Fermi level. In our case the fermi level shifts from -3.5171 eV (for pristine graphene) to -2.8091 eV (in K-doped graphene). With

increasing doping levels, the number of carriers increases which in turn increases electron-phonon coupling (EPC). This leads to superconductivity Figure 5.16 shows phonon band structure and density of states for K-doped graphene. If we compare the potassium-doped graphene with the pristine graphene, there are some new bands in the doped one Figure 5.16. This new created bands are near to the Fermi level and hence these are expected to create the superconductivity. Similarly if we compare the the PHDOS of pristine graphene and potassium-doped graphene, we can observed that the density of states (PHDOS) is increased around the Fermi level and this proofs that doping graphene with alkali adatoms induces superconductivity. Our results are also in good agreement with the results in the literature [1, 6].

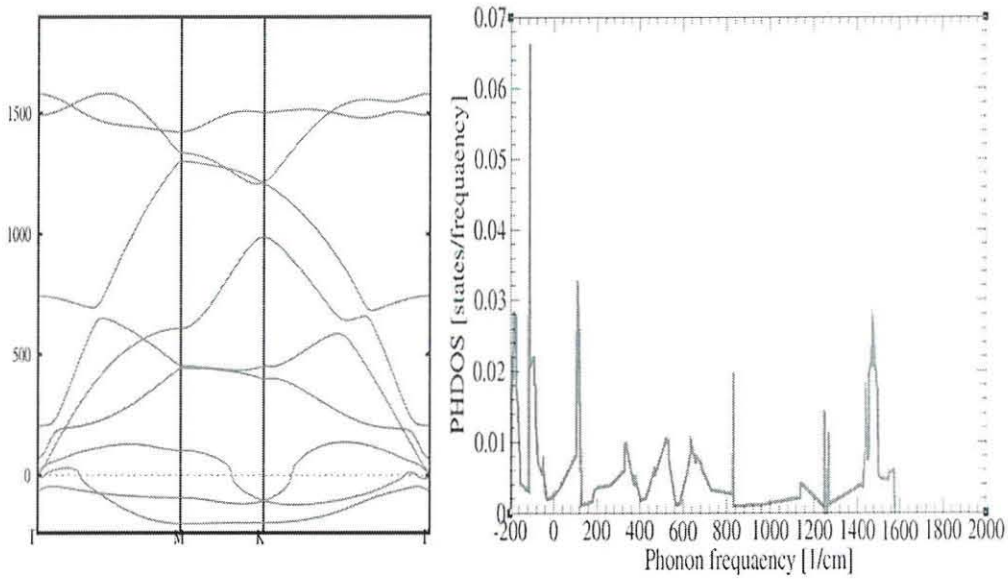

Figure 5.16: *Phonon band structure and density of states for K-doped graphene*

5.10 Calculations of electron-phonon couplings for pristine graphene

In this pristine graphene case, the coupling at the required frequancy (200 cm^{-1} – 900 cm^{-1}), which in this case 888.062cm^{-1} is completely zero. The coupling

is in the strong optical mode phonon modes, but by Equation 1.5 this strong modes diminish the coupling strength. So we need to induce coupling at this frequency. If we consider all the relevant frequencies and their corresponding coupling strength's, we found the sum of the frequencies by McMillan formula [37], $\sum_{qv} \lambda_{qv} = \lambda$, the result is 0.0000, at this point. The ω_{log} for this is $851.493 cm^{-1}$.

Table 5.1: *Phonon frequencies along with respective values of coupling for the pure graphene at the gamma point.*

R.No.	mode	ω (cm^{-1})	λ
1	ZA	44.103717	0.0000
2	TA	71.022711	1.0545
3	LA	71.022711	1.2921
4	ZO	888.061841	0.0000
5	TO	1619.050907	0.2300
6	LO	1619.050907	0.2365

5.11 Calculations of electron-phonon couplings for rubidium-doped graphene

In rubidium doped-graphene, due to the new electronic states at the Fermi level, the electron-phonon with the out-of-plane optical mode is created (ZO). Table 5.2 shows the phonon spectrum of rubidium-doped graphene. The first 9 rows are for the wave vector at zero (q = 0). At this wave vector the optical phonons are very strong hence from Equation 1.5, the coupling is negligible. Therefore this strong frequencies are not responsible for superconductivity. If we look row number six (which is the frequency of the intercalant atom), it is in the range of the EDOS and it has relatively good coupling (0.1714). When we perturb this material, we see that there are more phonon modes in the required range of energy. Phonon modes of row numbers 14, 15, 16 are in the range between 200 cm^{-1} and 900 cm^{-1}. So we can get more couplings from those modes. Here the strong optical modes become more softened. If we look the the electron-phonon coupling constant (EPCC) at the Γ-point, we observed that there is good EPIC (0.1714).

Table 5.2: *Phonon frequencies along with respective values of coupling of Rb-doped graphene at different wave vectors*

q = (0.00, 0.00, 0.00)				q = (0.25, -0.577, 0.00)		
♯	mode	$\omega_{ph} cm^{-1}$	Coupling	mode	$\omega_{ph} cm^{-1}$	Coupling
1	ZA	-19.374314	0.0000	ZA	-140.722234	-0.1459
2	TA	18.891995	0.0000	TA	94.36924	1.0997
3	LA	23.323979	0.0202	LA	110.409741	0.9645
4	ZA	61.572771	0.3099	ZO	471.657957	0.0083
5	TA	93.891611	0.0058	ZO	539.987636	0.0299
6	ZO	119.053290	0.1714	ZO	618.263242	0.0002
7	ZO	809.137492	0.0051	ZO	1344.375321	0.0022
8	TO	1560.638631	0.0698	TO	1348.981474	0.000
9	LO	1621.575760	0.0178	LO	1457.02888	0.0023
q = (0.00, 0.288, 0.00)				q = (0.25, 0.144, 0.00)		
1	ZA	-46.902188	-0.6010	ZA	-151.647220	-0.1656
2	TA	58.598601	0.8222	TA	-63.906340	-0.4657
3	ZO	182.257735	0.0341	LA	67.644749	0.4729
4	ZO	182.257735	0.0341	ZA	172.712787	0.0480
5	ZO	469.077709	0.0011	ZO	469.601141	0.0025
6	ZO	747.256759	0.0083	ZO	747.513537	0.009
7	ZO	799.226479	0.0014	ZO	794.474639	0.0047
8	TO	1526.052947	0.0043	TO	1504.597147	0.0126
9	LO	1609.887898	0.0027	LO	1603.489412	0.0068

5.12 Calculations of electron-phonon coupling for potassium-doped graphene

Electron-phonon coupling leads to attraction between electrons in a superconducting state [38, 39, 40]. More specifically, an electron polarizes the lattice, that is, it induces ionic motion which affects another electron. The process can be visualized as an exchange of phonons, such an exchange leads to an attraction between electrons. The important aspect of pairingsup is the logarithmic weakening of the Coulomb repulsion, which is related to the difference in the energy scales of the attractive and repulsive effects.

In order to interpret different experimental results in this area, a complete knowledge of the electronic structure, the phonon dispersion, and the electron-phonon interaction is required [41]. In graphene the electron-phonon coupling (EPC) between the π and π^* bands to different phonon modes is responsible for the peculiar properties observed in the experiments. Therefore to understand the possibility of superconductivity in potassium-doped graphene, we have calculated the strength of the electron-phonon coupling in this material.

As we can see from Table 5.3, the electron-phonon interaction for potassium-doped graphene is very large (0.3679) at the phonon frequency 204.247431 cm^{-1} which is at around the Fermi level. This electron-phonon constant coefficient clearly indicates that there is superconductivity of this potassium-doped graphene. And this is very similar case with previous works on superconductivity [43, 44, 45]. If we compare this result with the pristine case, which is zero at similar frequency, we can conclude that potassium-doped graphene becomes superconductor by phonon mediated coupling of cooper pairs [18]. Table 5.4 shows the coupling strength's for the calculated ω_{log} for frequency ranges in the electronic energies at the fermi level, that is from 100 cm^{-1} to 900 cm^{-1}.

As we can see from this table, the coupling strength at the Γ-point is largest with ω_{log} of 204.247cm^{-1} and with very nice T_c of 7.104097852 K which is one of the

Table 5.3: *Electron-phonon coupling at the respective phonon frequencies along with phonon line broadening in potassium-doped graphene. Data is presented for the wave vector zero (Gamma crystal Symmetry point)*

♯	mode	ω (cm^{-1})	coupling
1	ZA	-56.273625	-0.0004
2	TA	22.991416	0.0156
3	TA	26.402830	0.0009
4	LA	52.385021	0.0000
5	LA	79.993703	0.0000
6	ZO	204.247431	0.3679
7	ZO	736.879334	0.0000
8	TO	1547.1970014	0.1744
9	LO	1594.976987	0.1013

Table 5.4: *Average values of electron-phonon coupling and superconductivity critical temperature at thier respective phonon frequencies and at various symmetry points in the potassium-doped graphene*

♯	λ	ω_{log}	T_c
1	0.7358	204.247431	7.104097852
2	0.2004	358.875548044	0.00098955
3	0.2882	450.054988062	0.057882322
4	0.1676	295.940829843	0
5	0.225	456.093503484	0.00491059
6	0.1788	487.136405207	0
7	0.175	446.358951105	0

best critical tempratures of alkali atom doped superconductivity.

From the above tables of coupling and phdos spectra, it is clear that alkali doped graphene exhibit novel phenomenon of the enhanced electron phonon interactions in comparison to the pristine graphene. clearly, the enhanced interaction is menifested in the form of the softining of the phonon modes, especially the ZO modes among the doped graphene alon with high concentrations of electronic dos. Hence, the coupling, which is a paramount parameter for observing the superconductivity is found to increase correspondingly among doped graphene materials. The increase in coupling is more significant in K-graphene in comparison to Rb-graphene, however the enhancement of electronic dos is almost similar in both cases. This disparity can be interpreted from the coupling relation given

in the equation 1.7, in which square inverse mapping exists in between coupling and phonon frequency. It is to be noted from the table 5.3 that ZO modes of K-graphene is lower at frequencies in comparison to the ZO modes' values given in table 5.1 for Rb-graphne at their gamma points. This manifest in the form of enhanced superconductivity of K-graphene with higher critical temperature.

Chapter 6

Conclusion

Using ab-initio density functional theory (DFT) with plane-wave-pseudopotential implementations we first optimized the lattice constant of graphene supercell in doped (K, Rb) and undoped configurations along with other DFT parameters. This is followed by the simulations of their electronic band structures and density of states. Furthermore, we have used the density functional perturbation theory (DFPT) technique for the calculations of the vibrational frequencies of acoustic and optical phonon modes of the graphene in both doped and undoped states. A significant changes in the phonon spectra are obtained due to the effect of alkali atom doping on the vibration modes. The optical phonon frequencies of the graphene are found to be softened owing to alkali proximity for both the configurations of K and Rb graphene. Especially, the frequency of out-of-plane optical mode (ZO) has been found to softened significantly; the decrease in ω ZO values are 80 cm-1 and 150 cm-1 for the Rb and K doped graphene respectively. The effect of softening is further explored through the electron-phonon coupling by using linear response DFPT calculations that shows significant enhancements in the electron phonon interactions. Besides, we have observed the doping induced richness in the electronic band structure, electronic density of states and phonon density of states with a correlation among these properties. At the same time, we have shown that in pristine graphene the electron phonon interaction is negligible

as expected. While in potassium-doped graphene, we found it is 0.36779,which makes this material a good candidate for superconducting material. The critical temprature for K-graphene is found to be significant 7.1041 K. Although for rubidium-doped graphene, we found rich electronic states but the interaction coefficient is small with value of 0.1907 that is much smaller than potassium. This difference among the alkali doping induced coupling is attributed to the softening of ZO modes. Lastly, the prospects of doping of the graphene with alkali metals are discussed in detail in the thesis for exploring the superconductivity among them.

Bibliography

[1] Gianni Profeta, Matteo Calandra, Francesco Mauri, *Phonon-mediated superconductivity in graphene by lithium deposition*, Nature Physics, 8, 2181-2190, (2012)

[2] Daniel R. Cooper, Benjamin D'Anjou, Nageswara Ghattamaneni, Benjamin Harack,Michael Hilke, Alexandre Horth, Norberto Majlis, Mathieu Massicotte, Leron Vandsburger, Eric Whiteway, and Victor Yu, *Experimental Review of Graphene*, Condensed Matter Physics, 2012, 1-56, (2012)

[3] J.C. Charlier, P. C. Eklund J. Zhu, A. C. Ferrari, *Electron and Phonon Properties of Graphene: Their Relationship with Carbon Nanotubes*, Department of Physics, The Pennsylvania State University, 104, 673-709, (2008)

[4] Efthimios Kaxiras, *Atomic and Electronic Structure of Solids*,Cambridge University press, 1, 282-310, (2003)

[5] Kevin T. Chan,J. B. Neaton,Marvin L. Cohen, *First-principles study of metal adatom adsorption on graphene*, Physical Review B 77,10, 235430-235442, (2008)

[6] Matteo Calandra, Gianni Profeta, Francesco Mauri, *Superconductivity in metal-coated graphene*, Phys. Status Solidi, 12, 2544–2548, (2012)

[7] Junji Haruyama, *Superconductivity in carbon nanotubes*, Japan Science and Technology Agency, 33, 332-0012, (2010)

[8] Hubert B. Heersche, Pablo Jarillo-Herrero, Jeroen B. Oostinga, Lieven M.K. Vandersypen, Alberto F. Morpurgo, *Induced superconductivity in graphene* Solid State Communications, 143, 72–76, (2007).

[9] R.J. Wojciechowski, L. Kowalewski and M. Nogala, *Tunneling Charge Transport in Graphene-Based Superconductor Junctions* , Acta physica polonica , 121, 1-3, (2012)

[10] Huajun Qin, Junren Shi, Yanwei Cao, Kehui Wu, Jiandi Zhang, E. W. Plummer, J. Wen,4 Z. J. Xu,G. D. Gu, and Jiandong Guo, *Direct Determination of the Electron-Phonon Coupling Matrix Element in a Correlated System*, Physical Review Letters, 105, 256402-256406, (2010)

[11] Richard M.Martin, *Electronic structure:Basic theory and practical methods*, Cambridge University Press, 2, 10011-14222, (2004)

[12] Jenson, *Introduction to computational chemistry*, John Wiley and Sons, 2, 80-101, (2007)

[13] Andrew Gilbert, *Introduction to Computational Quantum Chemistry: Theory*, The Australian National University, (2007)

[14] S Kurth, Mal Marques, Eku Gross, *Density Functional Theory*, Elsvier LTD, 62, 395-402,(2005)

[15] R.A.Jishi , D.M. Guzman, *Theoretical Investigation of Two-Dimensional Superconductivity in Intercalated Graphene Layers* , Theor.Phys, 5, 703-716, (2011)

[16] Wolfram Koch, Max C. Holthausen, *A Chemist's Guide to Density Functional Theory*, Wiley-VCH, 2, (2001)

[17] P. Giannozzi, S. Baroni, N. Bonini, M. Calandra, R. Car, C. Cavazzoni, D. Ceresoli,G. L. Chiarotti, M. Cococcioni, I. Dabo, A. Dal Corso, S. Fabris, G. Fratesi, S. de Gironcoli, R. Gebauer, U. Gerstmann, C. Gougoussis, A.

Kokalj, M. Lazzeri, L.Martin-Samos, N. Marzari, F. Mauri, R. Mazzarello, S. Paolini, A. Pasquarello,L. Paulatto, C. Sbraccia, S. Scandolo, G. Sclauzero, A. P. Seitsonen, A. Smogunov, P. Umari, R. M. Wentzcovitch,, *QUANTUM ESPRESSO: A modular and open-sourcesoftware project for quantum simulations of materials*, version 5.0.1, J.Phys.:Condens.Matter 21, (2009)

[18] Matthias Einenkel and Konstantin B. Efetov, *Possibility of superconductivity due to electron-phonon interaction in graphene*, Institut fur Theoretische physic III, (2011), URL: http://www.core.kmi.open.ac.uk

[19] Cheol-Hwan Park,Feliciano Giustino,Marvin L. Cohen, and Steven G. Louie, *Electron-Phonon Interactions in Graphene:Bilayer Graphene and Graphite*, Nano letters, 8, 4229-4233, (2008)

[20] Normconserving Pseudopotentials , *URL:http://www.th.physik.uni-frankfurt.de* , Retrieved on May 17^{th}, (2013).

[21] Ultrasoft pseudopotentials, *URL:http://www.tcm.phy.cam.ac.uk* , Retrieved on May 18^{th}, (2013)

[22] Matteo Calandra, Francesco Maur, *Origin of superconductivity of $CaC_6$and of other intercalated graphites* , Phys. stat. sol. (b) 243, 13, 3458-3463, (2006)

[23] paolo Giannozzi, Stefano Baroni, *Handbook of Materials Modeling*, Springer, 2, 189-208, (2005)

[24] Mikhail I. Katsnelson, *Graphene: carbon in two dimensions*, Radboud University Nijmegen, 2, 6525-6544, (2006)

[25] David Vanderbilt, *Theory of Pseudopotentials* , The State University of Newjersey, 3, 1-28 , (2006)

[26] Quasi-Newton Method, *URL: http//www.en.wikipedia.org* , Retrieved on May 11^{th}, (2013)

[27] Mianqi Xue,Genfu Chen,Huaixin Yang,Yuanhua Zhu,Duming Wang,Junbao He,and Tingbing Cao, *Superconductivity in Potassium-Doped Few-Layer Graphene*, Journal of the American chemical society, 134, 6536-6539, (2012)

[28] Gabor Csanyi, P. B. Littlewood, Andriy H. Nevidomskyy, Chris J.Pickard, B. D. Simons, *The role of the interlayer state in the electronic structure of superconducting graphite intercalated compounds*, Cavendish Laboratory,UK, (2005)

[29] Omar Faye, *Metal Adatom Adsorption on Graphene Sheet:A First-principle Study*, The African Review of Physics, 7, (2012)

[30] *Rubidium properties*, URL: http://www.en.wikipedia.org, Retrieved on May 4^{th}, (2013)

[31] M.Farjam , H. Rafii-Tabar, *Energy gap opening in submonolayer lithium on graphene: Local density functionaland tight-binding calculations*, Shahid Beheshti University of Medical Sciences, 2, (2009).

[32] S. Piscanec, M. Lazzeri, F. Mauri, A.C. Ferrari, *Optical phonons of graphene and nanotubes*, The European Physical Journal, 148, 159–170, (2007)

[33] G D Sanders, A R T Nugraha, K Sato , J-H Kim, J Kono, R Saito, C J Stanton, *Theory of coherent phonons in carbon nanotubes and graphene nanoribbons*, J. Phys.: Condens. Matter, 25, 144201-144233, (2013)

[34] *Dissertation Mahdi Pourfath*, URL:http://www.iue.tuwien.ac.at, Retrieved on May 5^{th},(2013)

[35] Claudio Attaccalite1, Ludger Wirtz , Michele Lazzeri, Francesco Mauri and Angel Rubio1, *Doped graphene as tunable electron-phonon coupling material*, URL:http://www.arXiv.org cond-mat arXiv:1003.0995, (2010)

[36] A. Grüneis, C. Attaccalite, A. Rubio, D. V. Vyalikh, S. L. Molodtsov, J. Fink, R. Follath, W. Eberhardt, B. Büchner, and T. Pichler, *Electronic*

structure and electron-phonon coupling of doped graphene layers in KC8, Physical Review B, 79, 205106-205121, (2009)

[37] T. Cuk, D. H. Lu1, X. J. Zhou1, Z.-X. Shen, T. P. Devereaux, and N. Nagaosa , *A review of electron–phonon coupling seen in the high-Tc superconductors by angle-resolved photoemission studies*, phys. stat. sol., 242, 11– 29 (2005)

[38] Rasmita Sahoo and Rashmi Ranjan Mishra, *Phonon Dispersion of Graphene Revisited* , Journal of Experimental and Theoretical Physics, 114, 805–809, (2012)

[39] Patrick B. Benasutti, *Electronic and Structural Properties of Silicene and Graphene Layered Structures*, Wright State University, 1, 10-77, (2012)

[40] M.S.D Resselhaus, P.Eklund, *Phonons in carbon nanotubes*, Advances in physics, 49, 705 - 814, (2000)

[41] Pablo Buruset, William Javier Herrera, Alfredo Levy Yeyati, *Formation of Interface Bound States on a Graphene-Superconductor Junction in the Presence of Charge Inhomogeneities*, Scientific Research, 2, 35-41, (2013)

[42] J. Maultzsch, S. Reich, C. Thomsen,1 H. Requardt, and P. Ordejon , *Phonon Dispersion in Graphite*, Physical Review Letters 92, 7, 1-4, (2004)

[43] Rahul Nandkishore, L. S. Levitov,1 and A. V. Chubukov, *Chiral superconductivity from repulsive interactions in doped graphene* , Condensed Matter Mesoscale and Nanoscale Physics , 2 , (2011)

[44] J.-H. She, B. J. Overbosch, Y.-W. Sun, Y. Liu, K. E. Schalm, J. A. Mydosh, and J. Zaanen, *Observing the origin of superconductivity in quantum critical metals* , Physical Review B, 84, 144527 (2011)

[45] V.N. Popov, *Non-Adiabatic Phonon Dispersion of Graphene* , Bulg. J. Phys., 38, 72–84 , (2011)